Dynamic allocation of carbon storage and nutrient-dependent exudation in a revised genome-scale model of *Prochlorococcus*

Shany Ofaim[1,2*], Snorre Sulheim[1,3,4*], Eivind Almaas[3,5], Daniel Sher[2], Daniel Segrè[1,6,7¥]

1. Bioinformatics Program and Biological Design Center, Boston University, Boston, MA, USA
2. Department of Marine Biology, University of Haifa, Haifa, Israel
3. Department of Biotechnology and Food Science, NTNU-Norwegian University of Science and Technology, Trondheim, Norway
4. Department of Biotechnology and Nanomedicine, SINTEF Industry, Trondheim, Norway
5. K.G. Jebsen Center for Genetic Epidemiology, NTNU-Norwegian University of Science and Technology, Trondheim, Norway
6. Department of Biomedical Engineering, Boston University, Boston, MA
7. Department of Physics and Department of Biology, Boston University, MA

* These authors contributed equally to this work

¥ Corresponding author, Email: dsegre@bu.edu

Abstract

Microbial life in the oceans impacts the entire marine ecosystem, global biogeochemistry and climate. The marine cyanobacterium *Prochlorococcus*, an abundant component of this ecosystem, releases a significant fraction of the carbon fixed through photosynthesis, but the amount, timing and molecular composition of released carbon are still poorly understood. These depend on several factors, including nutrient availability, light intensity and glycogen storage. Here we combine multiple computational approaches to provide insight into carbon storage and exudation in *Prochlorococcus*. First, with the aid of a new algorithm for recursive filling of metabolic gaps (ReFill), and through substantial manual curation, we extended an existing genome-scale metabolic model of *Prochlorococcus* MED4. In this revised model (*i*SO595), we decoupled glycogen biosynthesis/degradation from growth, thus enabling dynamic allocation of carbon storage. In contrast to standard implementations of flux balance modeling, we made use of forced influx of carbon and light into the cell, to recapitulate overflow metabolism due to the decoupling of photosynthesis and carbon fixation from growth during nutrient limitation. By using random sampling in the ensuing flux space, we found that storage of glycogen or exudation of organic acids are favored when the growth is nitrogen limited, while exudation of amino acids becomes more likely when phosphate is the limiting resource. We next used COMETS to simulate day-night cycles and found that the model displays dynamic glycogen allocation and exudation of organic acids. The switch from photosynthesis and glycogen storage to glycogen depletion is associated with a redistribution of fluxes from the Entner-Doudoroff to the Pentose Phosphate pathway. Finally, we show that specific gene knockouts in *i*SO595 exhibit dynamic anomalies compatible with experimental observations, further demonstrating the value of this model as a tool to probe the metabolic dynamic of *Prochlorococcus*.

Introduction

Marine phytoplankton perform about one-half of the photosynthesis on Earth (Field et al., 1998). *Prochlorococcus* is one of the most abundant phytoplankton clades in the world's oceans and is estimated to produce about 4 Gt of organic carbon annually (Flombaum et al., 2013a). As such, these clades play a key role in a variety of ecosystems (reviewed by (Partensky and Garczarek, 2010; Biller et al., 2015)). Recent evolutionary studies suggested several evolved metabolic innovations contributing to high picocyanobacterial abundance in the harsh oligotrophic ocean waters, (Field et al., 1998) usually limited by several nutrients such as nitrogen, phosphorus, and iron. These innovations include a proteome that contains less nitrogen rich amino acids (Gilbert and Fagan, 2011), membranes that contain glyco- and sulfolipids rather than phospholipids (Van Mooy et al., 2006) and streamlining of the genome associated with outsourcing of important cellular functions to co-occurring organisms (Holtzendorff et al., 2008; Partensky and Garczarek, 2010; Morris et al., 2012; Ma et al., 2018a; Braakman, 2019).

Another innovation employed by these organisms is an increased metabolic rate that in turn manifest in the exudation of organic compounds (Braakman et al., 2017; Braakman, 2019), resulting in typically 2–50% of the carbon fixed by photosynthesis leaving the cell (Kujawinski, 2011; Thornton, 2014). Consequently, dissolved organic matter is an omnipresent component of natural waters. However, it is currently impossible to provide a universal chemical description of the dissolved organic matter (Kujawinski, 2011; Arrieta et al., 2015; Moran et al., 2016), partly because the exuded organic compounds differ between strains and environmental conditions (e.g. (Becker et al., 2014; Ma et al., 2018b)). Nevertheless, in general, phytoplankton exudate includes a small proportion of low-molecular weight compounds, such as organic acids, carbohydrates, and amino acids (Bertilsson and Berglund, 2014), as well as a larger proportion of complex, high-molecular weight compounds (Kujawinski, 2011).

Another strategy employed by these bacteria to manage their carbon budget is the internal storage of carbon in polymeric form, specifically, glycogen (Zinser et al., 2009; Reimers et al., 2017; Luan et al., 2019; Szul et al., 2019). Glycogen accumulates in the bacterial cell during the light hours and was recently suggested to have two primary roles; as energy storage in preparation for darkness and as a regulation strategy to manage high-light photosynthesis byproducts (Welkie et al., 2019). The allocation of glycogen is suggested to be tightly associated with the overflow metabolism hypothesis and also known to be widely affected by nutrient limitations (Damrow et al., 2016; Cano et al., 2018; Forchhammer and Schwarz, 2019; Szul et al., 2019). Importantly, the carbon fixed and released by phytoplankton is then used by heterotrophic organisms as a source of energy, whereas the heterotrophic bacteria may recycle nutrient elements and support the growth of phytoplankton in other ways, as suggested by the Black Queen Hypothesis (Amin et al., 2012; Morris et al., 2012; Moran et al., 2016; Cirri and Pohnert, 2019; Moran and Durham, 2019). Thus, carbon fixation, storage and release are tightly intertwined with microbial interactions and microbial ecosystem dynamics.

Quantitative models at various scales have provided critical insights into how ocean microbial ecosystems function, and how they are related to broader biogeochemical cycles (Braakman et al., 2017; Coles et al., 2017; Foster et al., 2018; Moradi et al., 2018). Most of these models represent organisms in terms of simplified stoichiometric reactions converting elements into biomass, thus making it possible to incorporate biological processes into dynamic-coupled Earth System models (Follows et al., 2007; Reid, 2011). The exponential increase in genomic information on marine organisms provides an opportunity to seek methods to link such detailed genome-scale information to biochemical flows (Coles et al., 2017). In recent years, genome-scale metabolic models (GEMs), combined with linear programming, have made it possible to produce testable predictions of metabolic phenotypes of individual organisms or microbial communities (Gu et al., 2019). This computational framework is based on the identification of individual enzymes and transporters in an organism's genome, and on simplifying assumptions that

bypass the need for kinetic parameters (Maarleveld et al., 2013; O'Brien et al., 2015; Casey et al., 2016; Kim et al., 2016; Reimers et al., 2017). While genome-scale modeling has proven to be a powerful approach in cyanobacterial model organisms such as *Synechocystis* sp. PCC 6803, *Synechococcus* elongatus PCC 7942 and *Prochlorococcus marinus* MED4 (Knoop et al., 2013; Broddrick et al., 2016; Casey et al., 2016; Yoshikawa et al., 2017), the exudation of organic compounds in phototrophic organisms has not been studied in detail through Flux Balance Analysis (FBA) or similar methods (Varma and Palsson, 1994; Orth et al., 2010). On the other hand, several examples exist of FBA-based predictions of exudation-mediated interactions between different species, including using the COMETS platform (Harcombe et al., 2014). In fact, FBA calculations also suggest that "costless" secretions (i.e. secretions that do not induce a fitness cost) might be quite common, and can support the growth of co-occurring organisms (Pacheco et al., 2018).

Experimental evidence and theoretical considerations indicate that *Prochlorococcus* exudes different metabolites in a way that strongly depends on environmental conditions (Dubinsky and Berman-Frank, 2001; Szul et al., 2019) as well as on the strain's genetic makeup (Becker et al., 2014; Roth-rosenberg et al., 2019). While GEMs can be used to predict these fluxes, they require modifications to deal with processes not usually considered in FBA, including: (a) the special nature of photon fluxes (which, unlike molecular fluxes, cannot easily be "shut off" at short time scales, (Dubinsky and Berman-Frank, 2001)); (b) the buffering role of intracellular storage molecules such as glycogen. The primary focus of this study is to obtain better knowledge of the potential metabolic effect of a combination of key nutrients (carbon, nitrogen, phosphorous and light) and carbon fixation rate on the allocation (including storage and exudation) of carbon in *Prochlorococcus* using a revised genome-scale metabolic model (Figure 1). We start by describing model revisions and updates to capture the current, most complete metabolic knowledge available for *Prochlorococcus*. Next, we use a variety of FBA approaches to uncover the potential relationships between a set of key nutrients, carbon storage and exudates in static and

dynamic (time dependent) settings. The implementation and use of these approaches improve our understanding of the intricate metabolic workings of *Prochloroccoccus* and provide insights on its storage and exudation trends under different environmental conditions.

Methods

Model update and curation

The *i*JC568 genome-scale reconstruction of *Prochlorococcus marinus subsp. pastoris str.* CMP1986 (referred to throughout the manuscript as MED4) as described by Casey et al. (2016), was used as the starting point for model enhancement. The update process started with an in-depth study of the reconstructed network and available knowledge not previously incorporated into the model of the organism. During this process, we ended up implementing the following specific steps of curation and update: (i) A key modification to the model was the decoupling between the glycogen storage flux and the biomass production. In standard stoichiometric reconstructions for FBA modeling (Thiele et al., 2011; Nogales et al., 2012; Feist et al., 2014; Broddrick et al., 2016; Monk et al., 2017; Kavvas et al., 2018), glycogen is listed as one of the biomass components, thus accounting for the carbon flux into storage. However, given the fixed stoichiometry of biomass composition, this classical implementation cannot account for the time-dependent storage and re-utilization of glycogen observed in picocyanobacteria. We thus removed the glycogen from the biomass function and streamlined the existing glycogen granule representation to a direct link between ADP-Glucose to the production of glycogen (Figure 1B). (ii) In addition to targeted refinement of selected reactions, we used the KEGG database (Kanehisa and Goto, 2000) to perform an extensive search of previously known but missing metabolic reaction annotations. Indeed, we found 354 reactions that could be potentially added to the existing network. To incorporate this knowledge, we developed a semi-automated algorithm (ReFill,

137 described below). (iii) We coupled the implementation of the algorithm with several steps of manual
138 curation. These included the addition of transports, such as that of hydrogen peroxide and ethanol,
139 known to diffuse across the cell membrane (Seaver and Imlay, 2001; Noreña-Caro and Benton, 2018),
140 and the addition of the complete Entner-Doudoroff pathway, that has recently been discovered in
141 cyanobacteria (Chen et al., 2016). Additionally, we performed a BLAST search (Supplemental material 1)
142 (Altschul et al., 1990) from which we identified 6PG-dehydratase (EC: 4.2.1.12) encoded by PMM0774,
143 thereby completing this pathway in the model reconstruction. (iv) The revised model was checked for
144 redox and elemental balance. Since the biomass function was based on experimental data (Casey et al.,
145 2016), it was not updated. In line with best practices, a *memote* quality assessment (Supplemental
146 material 2) (Lieven et al., 2020), as well as model files and a detailed changelog, are provided at
147 https://github.com/segrelab/Prochlorococcus_Model. All reactions added to iJC658 to form iSO595 are
148 found in Table S1 and modified reactions are found in Table S2.

149 ReFill algorithm

150 Following an extensive search of literature and the KEGG (Kanehisa and Goto, 2000), TransportDB
151 (Elbourne et al., 2017) and Metabolights (Haug et al., 2013) databases, we found a large number of new
152 or previously known but missing reaction, transporter and metabolite annotations. Adding large
153 amounts of data to an existing network might create new gaps and may give rise to new blocked
154 reactions and orphan metabolites. These, in turn, may affect optimization simulations. To add this
155 knowledge to the network in a controlled approach, we developed the semi-automated recursive
156 algorithm ReFill (Recursive Filler (of metabolic gaps)). The algorithm is based on the principle of using
157 diverse information, such as enzyme and reaction annotations, and experimental data (such as
158 metabolomics), to selectively increase the metabolic knowledge of an organism's existing curated
159 genome-scale metabolic network. ReFill makes use of a repository of reactions, in this case KEGG

reaction annotations for MED4 absent from the model, to construct all potential chains of reactions connecting two metabolites in the existing network. It systematically tests the potential of adding each new reaction and suggests adding it only if it can be a part of a chain in which all the metabolites are part of a path in the network (Figure 2). This prevents the creation of new orphan metabolites and potential blocked reactions that may lead to infeasible FBA solutions. The algorithm starts by selecting a reaction from the repository. It then inspects each metabolite in the reaction for presence in the existing network. In case a metabolite is not present, the set of available reactions is scanned for other reactions using this metabolite as a substrate or product. If such a reaction is found, it is added to the chain of potential reactions. The algorithm then iteratively expands the chain until either the repository is exhausted or all the metabolites in the most recent reaction added are present in the network. After all the possible chains of new reactions are expanded, the algorithm examines the connectivity of all the metabolites in each chain (See example in Figure 2B). Following the manual addition of transporters found through TransportDB (Elbourne et al., 2017) and Metabolights (Haug et al., 2013) (Study MTBLS567), using the ReFill algorithm, we updated reactions that belong to several different pathways, including metabolism of cofactors and vitamins, carbohydrate metabolism, amino acid metabolism and nucleotide metabolism. A complete list of added reactions can be found in Table S1. ReFill was coded in python 3.7 and generates MATLAB-compatible files formatted to be used with the COBRA MATLAB toolbox, including a list of suggested reactions to add and their gene-reaction rules. Other outputs include the added reaction chains and possible metabolic circuits that can be formed by these additions. All code (including ReFill) and model files are available on https://github.com/segrelab/Prochlorococcus_Model.

Parameter sampling

To study the effects of combinations of key nutrients on glycogen production and exudation in the *i*SO595 model we focused on four parameters representing the uptake fluxes of light, bicarbonate, ammonium, and phosphate. Light and inorganic carbon (bicarbonate) are the substrates for photosynthesis, whereas nitrogen and phosphorus limit the growth of *Prochlorococcus* in large regions of the world ocean (Davey et al., 2008; Moore et al., 2013; Saito et al., 2014), and nutrient limitation is likely to influence the exudation of fixed carbon (Dubinsky and Berman-Frank, 2001). We sampled 10,000 different environmental conditions by drawing random values from uniform distributions of these four parameters. The range of each parameter was based on physiologically relevant ranges we extracted from the literature and on the requirement that each range covers important phase transitions, such as nutrient and light limitations (Table S3). Light flux was converted from micromole quanta m^{-2} sec^{-1} to mmol $gDW^{-1}h^{-1}$ similarly to (Nogales et al., 2012) using 8% photosynthesis efficiency rate (Zinser et al., 2009). All parameter uptake fluxes are described in FBA compatible units (mmol $gDW^{-1}h^{-1}$), corresponding values in biogeochemistry relevant units are illustrated in Table S3. As MED4 is a photoautotroph, it is exposed to a constant stream of light during daylight hours. The bacterium is then forced, or 'pushed', to fix carbon even when there is not enough of other elements, such as nitrogen or phosphate, to combine the fixed carbon into biomass. To capture this phenomenon *in silico* we developed a 'push'-FBA framework where we fixed both upper and lower uptake rates of light and bicarbonate (Figure 1A). For the other sampled nutrients, ammonium and phosphate, we defined standard FBA bounds where the maximal uptake rate was set to the sampled value and the lower bound was set to zero. Note that, we only considered uptake of sulfur in the form of sulfate (not hydrogen sulfide), and no upper limit was set for the uptake of sulfate because of its abundance in seawater. The maximum rate of RuBisCO (R00024) was fixed to 4.7 mmol gDW^{-1} h^{-1}, as previously reported (Casey et

al., 2016). Before sampling we blocked a set of artificial exchange reactions that were added in the previous version of the model, most likely to allow export of dead-end metabolites that would otherwise limit flux feasibility (Table S4). Subsequently, we removed all unconditionally blocked reactions in the model to speed up computations. For each random sample, we first tested the model for feasibility using FBA (Varma and Palsson, 1994). If the solver returned a solution that was feasible and optimal, we further calculated optimal fluxes with parsimonious FBA (Lewis et al., 2010), and determined the range of possible fluxes at optimum with Flux Variability Analysis (FVA) (Gudmundsson and Thiele, 2010). Exchange fluxes from FBA, parsimonious FBA and FVA were recorded and used in subsequent analyses. All environmental sampling and calculations were performed using CobraPy (Ebrahim et al., 2013) and GUROBI 8.1.1 (Gurobi Optimization, Inc., Houston, TX, USA). The python script used to run the environmental sampling is available in the GitHub repository (https://github.com/segrelab/Prochlorococcus_Model).

Statistical analysis of the sampled spaces

We sampled 10,000 different environmental conditions based on the flux ranges described above, and analyzed the results of FBA optimization, with the goal of characterizing the distribution of specific import/export fluxes and the correlations between different fluxes. To that end, we calculated Pearson correlations between reaction fluxes in the sampling data using the python (version 3.7) Pandas package version 1.0.3 (McKinney, 2010). While negative values are normally used to define uptake in FBA, we converted them to positive values for the uptake of light, bicarbonate, phosphate, ammonium, and sulfate when calculating correlations to ease interpretation of the results. We also performed hierarchical clustering using the Nearest Point Algorithm in SciPy (Virtanen et al., 2020) to sort the order of the compounds in the correlation matrix. We performed dimensionality reduction on normalized reaction fluxes using the T-distributed Stochastic Neighbor Embedding (t-SNE) method (Maaten and

Hinton, 2008) in Scikit-learn (Pedregosa et al., 2011) with perplexity of 50 and 3000 iterations. The reaction fluxes were normalized to [-1,1] by dividing by the maximum absolute flux of each reaction. Finally, the t-SNE transformed data was clustered using HDBSCAN (McInnes et al., 2017) with a minimum cluster size of 200. Transport of inorganic ions, water, and protons were not considered when calculating correlations, dimensionality reduction or clustering. We also discarded transport reactions with no absolute flux value above 10^{-3} mmol gDW^{-1} h^{-1} in any of the environmental samples.

Dynamic modelling of light absorption during the diel cycle in COMETS

Cyanobacteria follow a diel cycle. To capture this dynamic behavior, we extended the Computation Of Microbial Ecosystems in Time and Space (COMETS) platform (Harcombe et al., 2014), and developed a module for diurnal-cycle simulations allowing oscillations of light intensity and light absorption. Attenuation of light through each grid cell was modelled using the Beer-Lambert law, as described previously (Yang, 2011; Gomez et al., 2014):

$$I(t,z) = I_0(t)e^{-(a_w + a_{dw}X)z} \quad (1)$$

Here, $I(t,z)$ is the light irradiance given in mmol photons m^{-2} s^{-1}, t is the time, z is the depth (from the top of the grid cell), a_{dw} is the cell- and wavelength-specific absorption coefficient given in m^2 gDW^{-1}, a_w the absorption coefficient of pure water given in m^{-1}, X the biomass concentration in gDW m^{-3}, and $I_0(t)$ time time-dependent incident light irradiance at the top of the grid cell. In the current version, we simplified the process by assuming that the light irradiance is either monochromatic or a sum of the total light bandwidth, and the absorption coefficient should match the wavelength(s) of the light source. The total light attenuation (ΔI) through a grid cell of thickness Δz is then

$$\Delta I(t) = I(t,0) - I(t,\Delta z) = I_0\left(1 - e^{-(a_w + a_{dw}X)\Delta z}\right) \quad (2)$$

The light absorbed by the cells is a fraction of the total light attenuation, i.e.

$$I_{abs}(t) = \frac{\Delta I(t) \cdot a_{dw}X(t)}{a_w + a_{dw}X(t)}. \quad (3)$$

The total number of photons absorbed per dry cell weight ($\Phi(t)$) in mmol photons $gDW^{-1}\ s^{-1}$ by the cells within a grid cell of thickness Δz, volume *V*, and surface area *A* is then

$$\Phi(t) = \frac{I_{abs}(t) \cdot A}{X \cdot V} = \frac{I_0(t) \cdot A}{X \cdot V}\frac{a_{dw}X(t)}{a_w + a_{dw}X(t)}\left(1 - e^{-(a_w + a_{dw}X)\Delta z}\right). \quad (4)$$

For all COMETS simulations presented here we have used monochromatic light at 680 nm with a calculated biomass-specific absorption coefficient a_{dw} as previously described (Morel and Bricaud, 1981; Bricaud et al., 2004). Briefly, the biomass-specific absorption is the weighted sum of the absorption coefficients of the light-absorbing pigments divinyl-chlorophyll A and B, since none of the other pigments in *Prochlorococcus* absorb light at 680 nm. Additionally, to account for the discrete distribution of chlorophyll into separate cells, the absorption coefficient is scaled by the packaging factor. All coefficients used to calculate light attenuation and absorption are provided in Table 1.

Table 1: Coefficients and values used to calculate light absorption in COMETS.

Symbol	Description	Value	Unit	Reference
λ	Wavelength	680	nm	
a_w	Absorption coefficient of water at 680 nm	0.465	m^{-1}	Pope and Fry, 1997
a_{dw}	Biomass-specific absorption coefficient	0.285	$m^2\ gDW^{-1}$	

$a_{dvchl\text{-}A}$	Absorption coefficient of divinyl-chlorophyll A at 680 nm	0.0184	m^2 (mg dvchl-A)$^{-1}$	Bricaud et al., 2004
$a_{dvchl\text{-}B}$	Absorption coefficient of divinyl-chlorophyll B at 680 nm	0.0018	m^2 (mg dvchl-B)$^{-1}$	Bricaud et al., 2004
$c_{dvchl\text{-}A}$	Amount of divinyl-chlorophyll A in	0.0163	g dvchl-A gDW^{-1}	Casey et al., 2016
$c_{dvchl\text{-}B}$	Amount of divinyl-chlorophyll B	0.0013	g dvchl-B gDW^{-1}	Casey et al., 2016
d	Average diameter of MED4	0.6	µm	
n'	Imaginary part of the refractive index at 675 nm	0.01377		Stramski et al., 2001
Q*	Packaging effect at 680 nm	0.945		

The changing light conditions throughout a diel cycle was modelled as

$$I_0(t) = A \max\left(\sin(\omega t), 0\right), \tag{5}$$

where the angular frequency is $\omega = \frac{2\pi}{T}$.

Following the development of the diel cycle simulation capability in COMETS we set out to dynamically simulate the growth of MED4. Since the nutrient uptake follows Michaelis–Menten kinetics, we estimated the kinetic parameters V_{max} and K_m using a heuristic approach from experimental data (Grossowicz et al., 2017), first by finding the range of possible parameter combinations corresponding to the gross growth rate of 0.5 d^{-1} (Figure S1A), and secondly by comparing predicted growth and ammonium depletion with the experimental time-series cultivation data (Figure S1B). The estimated parameters were used in the remaining dynamic FBA simulations in COMETS. Finally, to simulate the dynamic storage and consumption of glycogen we applied a multiple objective approach consisting of

the following four steps: (1) Maximization of the flux through the non-growth associated maintenance reaction. Note that, this reaction has an upper bound of 1 mmol gDW^{-1} h^{-1} (Casey et al., 2016) In contrast to standard practice, where one uses a lower bound for the non-growth associated maintenance reaction, this method provides a more realistic scenario where the organism continues to consume resources trying to keep up cellular maintenance even at zero growth; (2) Maximization of growth; (3) Maximization of glycogen production (storage); and (4) Parsimonious objective which minimizes the sum of absolute fluxes. To simulate nitrogen-abundant and nitrogen-poor growth conditions, we used the PRO99 medium with standard (800 µMol) and reduced (100 µMol) ammonium concentration, as previously described (Grossowicz et al., 2017). Light availability was modelled as described in Equation 5, with an amplitude of 40 µmol Q m^{-2} s^{-1} and a period of 24 hours. All parameter values used in the COMETS simulations are given in Table S5. All Dynamic growth simulations were performed using COMETS v.2.7.4 with the Gurobi 8.1.1 solver, invoked using the associated MATLAB toolbox (https://github.com/segrelab/comets-toolbox).

Simulating growth of knockout mutants

Simulations of the knockout mutants where performed by constraining the flux to zero for the reactions catalyzed by the enzymes encoded by *glgC* (PMM0769) and *gnd* (PMM0770), respectively. For *glgC*, the reaction is glucose-1-phosphate adenylyltransferase (R00948) and for *gnd* the two reactions are $NADP^+$ and NAD^+ associated 6-phosphogluconate dehydrogenases (R01528 and R10221). We then used dynamic FBA in COMETS with PRO99 medium (Moore et al., 2007) with limited ammonium and diel light conditions to simulate growth over 7 days. We included an arbitrarily derived death rate of 0.1 d^{-1} (Grossowicz et al., 2017) in these simulations. The growth curves where qualitatively compared with

experimental data from Shinde and co-workers (Shinde et al., 2020). The model parameters are given in COMETS parameter and model files in https://github.com/shashany/iSO595/tree/master/COMETS_files.

Results and Discussion

Model curation and update

Prochlorococcus fixes carbon through photosynthesis during daytime. Fixed carbon that is neither used for cell growth nor stored in the form of glycogen is exuded. Here, we set out to study dynamic changes in the carbon allocation and storage mechanisms in MED4 using a genome-scale metabolic modelling approach. To that end, we first re-curated and updated the available *i*JC586 model (Casey et al., 2016), as described in detail in the Methods section. The update involved the development of a new semi-automatic algorithm (ReFill), which can be broadly applied to other reconstructions (Methods). Concurrently, we introduced a revised mechanism for carbon storage, effectively treating glycogen as an independent component of biomass. This configuration makes it possible for glycogen to be accumulated and depleted at variable rates (Figure 1), aligning with the overflow metabolism hypothesis (Szul et al., 2019; de Groot et al., 2020). Other key modifications induced by the ReFill algorithm and subsequent manual curation (see Methods) include the completion of the Entner-Doudoroff (ED) pathway, recently discovered in cyanobacteria (Chen et al., 2016) and proposed as the primary *Prochlorococcus* glucose metabolism pathway under mixotrophic conditions (Biller et al., 2018), but see (Muñoz-Marín et al., 2020). Additional revisions focused on the exudation of fixed carbon products from the cell and included various transports such as pyruvate, fumarate, citrate, ethanol, various nucleotides and hydrogen peroxide as well as metabolites found in both the endo- and exo- metabolome of *Prochlorococcus* (Metabolights study MTBLS567). The end product of our revision, reconstruction

322 iSO595, has 595 genes, 802 metabolites and 994 reactions, i.e. 27 genes, 123 metabolites and 196
323 reactions more than the previous version, *i*JC568 (Figure 1D).
324

325 Carbon fixation and storage is affected by nutrient uptake rate

326 *Prochlorococcus* thrive in oligotrophic environments (Johnson et al., 2006), where, in surface waters, its
327 growth and carbon fixation rates are usually limited by the abundance of nitrogen, phosphate or iron
328 (Krumhardt et al., 2013; Szul et al., 2019). Deeper in the water column *Prochlorococcus* growth becomes
329 limited by light (Vaulot et al., 1995). We set out to explore the combined effect of different levels of light
330 and nutrients on carbon fixation, storage and exudation. Similarly to Phenotypic Phase Plane analysis
331 (Edwards et al., 2002), we sought a global perspective of metabolism in this multi-parameter spaces
332 while explicitly taking into account the fact that the inflow of light and bicarbonate may not be easily
333 controllable by the cell, and that *Prochlorococcus* may need to deal with excess amounts of fixed carbon.
334 Thus, in contrast to normal FBA where the uptake of metabolites is constrained by an upper bound, we
335 introduced a 'push- FBA' approach (Figure 1A), in which the influx of bicarbonate and light have a fixed
336 imposed value (See Methods and Table S3 for specific values used). This approach attempts to mimic
337 implications of photosynthesis, in which light is the driving force. Once photons are absorbed by the
338 chlorophyll, the energy must be used to produce ATP and reducing power, otherwise it is dissipated in
339 ways that may cause cell damage (Long et al., 1994). This subtle difference in applied constraints has
340 major effects on model predictions. While flux rearrangement is usually viewed as a consequence of
341 environmental nutrient limitations, the results of this analysis shows that a substantial rewiring of fluxes
342 is caused by this imposed excess of fixed carbon as well.
343 To understand how different combinations of environmental parameters (availability of nitrogen,
344 phosphate, light and bicarbonate) affect the way *Prochlorococcus* can manage its carbon budget, we
345 implemented FBA under 10,000 randomly sampled growth environments. Overall, this sampling analysis

346 demonstrated that the exudation of organic acids, amino-acids and nucleobases/nucleosides, as well as
347 the extent of glycogen storage, are strongly modulated by environmental factors (Figure 3). To observe
348 the full range of possible optimal solutions per sample, we implemented and compared different flux
349 balance analysis methods, including flux variability analysis (FVA) and parsimonious FBA (pFBA). These
350 two methods provide complementary insight: FVA estimates the range of possible values for the flux of
351 each reaction at the optimum, providing insight into the structure of the phenotypic space at maximal
352 growth rate. In contrast, pFBA, by minimizing the sum of fluxes at optimality, generates flux predictions
353 less likely to involve unrealistic loops, and thus potentially provides predictions closer to experimental
354 values (Lewis et al., 2010). Together, these two FBA methods help analyze the solutions of our high-
355 dimensionality dataset.
356 Our predictions simulate the metabolic effects and variability in glycogen production modulated by
357 environmental constraints (Figure 3). Glycogen production was observed only above light levels of 50
358 mmol gDW^{-1} h^{-1} (corresponding to 7.5 micromole quanta m^{-2} sec^{-1}), and decreased as ammonium and
359 phosphate concentrations increase, in agreement with previous studies (Szul et al., 2019). Interestingly,
360 FVA consistently predicted the glycogen production range minimal value to be zero across all samples.
361 This implies that glycogen storage is possible, but not necessary to achieve optimal growth in the
362 feasible solution space. This was also the case in the more stringent pFBA analysis, indicating that while
363 metabolism may be a strong modulator of glycogen metabolism, more types of regulation, not
364 accounted for in FBA, are involved. One example of such regulation may be allosteric regulation of ADP-
365 glucose pyrophosphorylase by 3-phosphoglycerate (Iglesias et al., 1991), possibly in combination with
366 redox regulation (Díaz-Troya et al., 2014). Specific regulation aimed at tuning up glycogen storage may
367 also occur at the transcriptional level, e.g. by multiple transcription factors previously suggested to be
368 involved in the regulation of glycogen metabolism in fluctuating environments (Luan et al., 2019).

369 The range of possible rates of glycogen production (through FVA) displays a bell-shaped bicarbonate
370 dependent distribution, indicating low storage of glycogen (zero flux) under both low and high uptake
371 rates of bicarbonate. When bicarbonate uptake rates are low, all available carbon is diverted into
372 growth. The reduced glycogen storage at high bicarbonate uptake, when RuBisCO is saturated, seems to
373 be caused by the increased ATP demand associated with the conversion of bicarbonate to exudation-
374 products, since the onset and rate of change of this trade-off is modulated by the ATP availability, as
375 demonstrated by phenotypic phase planes analysis (Figure S2). This agrees with recent work suggesting
376 that *Prochlorococcus* use available ATP to drive pathways to saturation by shifting reaction directions
377 towards favoring dephosphorylation of ATP to ADP, disrupting the cellular ATP/ADP ratio and increasing
378 the metabolic rate of the cell by pushing forward ATP consuming reactions, until it is restored. Together
379 with organic carbon exudation this strategy allows for growth in lower nutrient concentrations
380 (Braakman, 2019).
381 We next sought to explore the effect of combinations of key nutrients on storage and exudation
382 patterns in our sampling spaces. To explore the strongest trends, we chose to employ a high stringency
383 approach and use only our set of pFBA results. Due to the nature of pFBA, any exudation observed in
384 this analysis could not be easily removed without imposing a cost on growth. To that end, we visualized
385 the data using t-SNE clustering (Figure 4A) on our pFBA set of results. We observed 6 typical phenotypes
386 (clusters) rising out of the sampling spaces (Figure 4). These 6 phenotypes are characterized by subtle
387 differences in combinations of environmental parameters, yielding significantly different exudation
388 patterns. Generally, we observed the highest biomass value in phenotype 5, and the lowest in
389 phenotype 4. All key nutrient uptake rates were highly variable (ranging from 33 to 44% variability).
390 Phenotype 1 is characterized by high light, bicarbonate, a maximum RuBisCO flux (indicating maximal
391 photosynthesis rate) but low nitrogen uptake. Additionally, we observed high exudation of pyruvate
392 coming from the pentose phosphate and Entner-Doudoroff pathways. Both are alternative routes

coming out of carbon fixation (Waldbauer et al., 2012; Chen et al., 2016). Together with a low biomass value, this phenotype might indicate a scenario of exudation due to overflow metabolism.

The two largest clusters (number 2 and 3), tie together high and low light, carbon and nitrogen uptake rates, and different exudation patterns. Interestingly, phenotype 3 (high light) showed exudation of fumarate and malate while phenotype 2 (low light) did not. Recent work suggested that, in high light conditions, fumarate is generated through oxaloacetate and malate creating a broken acyclic form of the TCA cycle, while in the dark, fluxes are diverted into forming the cyclic form of it. This low light form of the TCA cycle is then active and works towards energy generation (Xiong et al., 2017). Similarly, we observed two forms of the TCA cycle in the high and low light phenotypes (2 and 3 respectively) with a difference in the direction of one reaction (KEGG R00342, Figure S3). Phenotype 2, describing low-light conditions, showed the L-Malate/oxaloacetate balance to shift in favor of oxaloacetate, completing the route towards 2-Oxoglutarate, a key metabolite known to act as a starvation signal and modulator of the C/N balance in cyanobacteria (Domínguez-Martín et al., 2018; Zhang et al., 2018), and subsequently into energy generation. On the other hand, Phenotype 3, describing high light conditions, showed the L-Malate/oxaloacetate balance to shift in favor of L-Malate and away from the formation of 2-oxoglutarate. In both phenotypes fumarate is converted to L-Malate. While in Phenotype 2 it is fed into a semi-cyclic form of the TCA cycle, fumarate is partly exuded and partly converted to L-malate in phenotype 3, in agreement with overflow metabolism.

We observed a similar TCA cycle flux distribution in phenotype 4 leading to high exudation of L-Malate. Interestingly, Phenotype 1 and 4 are comparable in all key nutrients except light (High in phenotype 1 and low in phenotype 4). As a result of an in-depth flux distribution analysis, we observed a reaction direction change in UDP-glucose:NAD+ 6-oxidoreductase [R00286, EC 1.1.1.22, PMM1261] between the two phenotypes. In phenotype 4 this reaction shifted towards the creation of UDP-glucose, a precursor for the production of glycogen (Due to the high stringency of this analysis we did not observe the direct

417 formation of glycogen). In phenotype 1, this reaction favored the formation of UDP-glucuronate which
418 in turn was diverted into the formation of amino sugars. These phenotypes may correlate to the 12:00
419 (phenotype 1) and 16:00 (phenotype 4) scenarios described in (Szul et al., 2019). Finally, Phenotypes 5
420 and 6 may represent a high-light nutrient-rich environment resulting in a high biomass value.
421

422 Nutrient uptake rates modulate exudation of organic compounds

423 The use of genome-scale metabolic models captures a comprehensive picture of the metabolic
424 processes taking place in the cell, including those that lead to metabolite exudation. From the random
425 sampling of environmental conditions, we identified conditions in which organic acids must be exuded.
426 This was noticeable by a non-zero lower bound of the FVA region (Figure 3). Interestingly, organic acids
427 were more likely to be exuded when the growth became limited by phosphate or nitrogen. Since
428 *Prochlorococcus* is known to thrive in oligotrophic ocean gyres where nitrogen or phosphate is limited
429 (Partensky et al., 1999; Flombaum et al., 2013b), this represents a likely natural phenotype, and as such,
430 supports previous findings (Szul et al., 2019). Costly metabolites, essential for cell survival and growth,
431 such as amino acids, nucleobases and nucleotides, tend to be exuded in nitrogen and carbon rich
432 conditions and might be a result of overflow metabolism (Cano et al., 2018; Pacheco et al., 2018). To
433 explore this phenomenon in further detail, we looked into exudation patterns of specific metabolites as
434 a function of key nutrient limitations (Figure 5). Of the environmental factors, the uptake of nitrogen
435 (ammonium) is a decisive factor differentiating between exudation of organic acids or amino acids.
436 While it is positively correlated with the exudation of nitrogen-rich compounds such as amino acids, it is
437 negatively correlated with exudation of organic acids and glycogen. Additionally, glycogen formation is
438 positively correlated with the exudation of malate, citrate, fumarate and succinate, which are most of
439 the TCA cycle constituents. This is in line with previous findings suggesting the re-direction of carbon
440 metabolism towards the formation of macromolecules (including glycogen) in nitrogen limiting

441 conditions (Forchhammer and Selim, 2019; Szul et al., 2019). Thus, our reconstruction captured known
442 possible aspects of the carbon/nitrogen balance in *Prochlorococcus*.
443 Finally, we observed a general pattern of strong positive correlations between amino acids, nucleobases,
444 nucleosides, as well as a range of other compounds. In an interesting deviation from this general
445 pattern, L-Aspartate showed a decreased correlation with other exudates. L-Aspartate, together with its
446 role in protein nucleic acid biosynthesis, can serve as a precursor for nitrogen storage metabolites such
447 as polyamines (Szul et al., 2019). Indeed, we observed a slightly stronger correlation between L-
448 Aspartate and the uptake of nitrogen compared to other amino acids. Finally, In contrast to other amino
449 acids, L-Aspartate is negatively correlated with light uptake and hydrogen peroxide exudation. Hydrogen
450 peroxide is produced from L-Aspartate and oxygen by L-aspartate oxidase [R00481, EC 1.4.3.16,
451 PMM0100]. L-amino acid oxidases have been previously described in cyanobacteria and have been
452 related to the use of amino acids as carbon sources (Campillo-Brocal et al., 2015). The production of
453 hydrogen peroxide is also strongly correlated with light, a result consistent with the expectation that
454 reactive oxygen species are created during photosynthesis.
455

456 Dynamic allocation of carbon storage

457 Nutrient and light limitations are well-known modulators of carbon storage in *Prochlorococcus* (Zinser et
458 al., 2009; Szul et al., 2019). Recent work has suggested the storage of carbon to be one of the major
459 metabolic tasks during the day-night cycle (Cano et al., 2018; Szul et al., 2019; Shinde et al., 2020).
460 Sampling 10,000 environmental conditions showed that glycogen production decreased at lower light
461 intensities and was less saturated at higher rates (Figure 3). To explore other time-modulated trade-offs
462 and trends related to carbon storage, we performed *in silico* dynamic FBA diel-cycle simulations using
463 the Computational of Microbial Ecosystems in Time and Space (COMETS) platform (Mahadevan et al.
464 2002; Harcombe et al. 2014). COMETS relies on kinetic information such as K_m and V_{max} to simulate the

spatial growth and exudation patterns of microbes in a simulated discretized time course. To improve the accuracy and biological relevance of our simulations we used kinetic constants either obtained from experimental measurements reported in the literature (Krumhardt et al., 2013; Hopkinson et al., 2014) (Table S3) or from fitting model simulations to measured growth and depletion of ammonium rates (Grossowicz et al., 2017). We found K_m and V_{max} values of 0.39 mM and 0.9 mmol gDW^{-1} h^{-1} for the uptake of ammonium to best fit the experimental data (Grossowicz et al., 2017) (Figure S1). Surprisingly, the estimated K_m value is 3 orders of magnitude larger than previous estimates (Grossowicz et al., 2017), indicating some uncertainty in this estimate that may be affected by the choice of method for calculating this value.

Since the tight coupling between carbon and nitrogen metabolism in cyanobacteria is known to influence carbon allocation and storage (Zhang et al., 2018; Szul et al., 2019), it was chosen as a case study. As such, we focused in more detail on the dynamic changes in metabolism in nitrogen-abundant and nitrogen-poor media, as previously defined (Grossowicz et al., 2017). Specifically, we set out to explore glycogen production and consumption with COMETS in these conditions (Figure 6). We did not observe glycogen storage in nitrogen-abundant simulations. One explanation for this may arise from the limitations of the platform. The modelling framework is based on linear programming to optimize an ordered set of assumed cellular objectives, glycogen is only stored when there is excess energy and carbon available, which is the case when the growth is nitrogen limited. Another limitation that might affect glycogen storage in these simulations might involve other types regulatory mechanisms not usually accounted for in dynamic FBA. The addition of regulatory layers, such as proteomics data (Reimers et al., 2017), or more specifically tailored objective functions could lead to smaller but nonzero generation of glycogen also during nitrogen-rich conditions.

In agreement with previous work (Szul et al., 2019), under nitrogen-limiting conditions, glycogen accumulates throughout the day and is subsequently used to support respiration and growth during the

night (Figure 6A). However, the predicted glycogen storage is not sufficient to support neither growth nor cellular maintenance during the night and may explain the reported increased death rate during night time (Zinser et al., 2009; Ribalet et al., 2015). Interestingly, the model predicts consumption of glycogen during dusk to increase growth when photosynthesis is declining (Figure 6), closely resembling observations in *Synechococcus,* in particular for the *ΔkaiC* mutant with a dysfunctional circadian clock (Diamond et al., 2015).

The switch from photosynthesis at daytime to glycogen consumption at nighttime is reflected in the metabolic shifts observed in key pathways (Figure 6B). Interestingly, we observed higher fluxes through the Calvin cycle in nitrogen-poor conditions. This difference may be caused by the increased ATP demand necessary to support higher growth rates in nitrogen-abundant conditions. Additionally, our simulations predicted that the use of the Entner-Doudoroff pathway during photosynthesis creates precursor metabolites for growth during light hours, and a shift to the Pentose Phosphate Pathway (PPP) during nighttime. This trend might occur as an alternative for generating NADPH (Figure S4). Upregulation of the PPP enzymes during dusk and the first half of the night time was also observed in the proteome of *Prochlorococcus* (Waldbauer et al., 2012). Several enzymatic transformations participate in both the Calvin cycle and the PPP, although in opposite directions (Waldbauer et al., 2012). These transformations were captured in our simulations, specifically as demonstrated by transketolase (Figure 6B). Additionally, the consumption of glycogen during nighttime leads to exudation of pyruvate and formate (Figure 6C). This prediction is supported by previous observations; formate is exuded when phosphonates are metabolized in the closely related strain *Prochlorococcus marinus* MIT9301 (Sosa et al., 2019) and pyruvate is exuded when fixed carbon is consumed in *Synechococcus* elongatus PCC 7942 and *Synechocystis* sp. PCC 6803 (Carrieri et al., 2012; Benson et al., 2016).

The shift from photosynthesis and carbon fixation to glycogen catabolism is also associated with a switch in production and consumption of energetic cofactors (Figure S3). Generation of ATP is

513 performed concomitantly by ATP synthase in both the thylakoid membrane and the periplasmic
514 membrane during photosynthesis. The periplasmic ATP synthase is first driven by reduced cofactors
515 (NADPH) generated by the electron transport chain in the light-dependent part of photosynthesis
516 (Figure S3). ATP is consumed by two separate processes: growth- and maintenance-associated reactions
517 reach a threshold once growth is limited by the nitrogen abundance, while the recycling of precursors
518 for the Calvin cycle follows the shape of light absorption throughout the day. In agreement with
519 previous work (Park and Choi, 2017), our model predicted higher rates of NADPH production than
520 NADH.

521 Next, we explored the ability of our model to dynamically capture biologically relevant phenotypes by
522 performing dynamic FBA simulations of knock-out mutants in *Prochlorococcus,* focusing on two gene
523 deletions disrupting different parts of glycogen metabolism. Δ*glgC* breaks synthesis of ADP-glucose and
524 thus the storage of glycogen and Δ*gnd*, knocking out 6-phosphogluconate dehydrogenase, a key
525 reaction in the Pentose Phosphate pathway found to fuel the Calvin cycle with precursor metabolites
526 during the onset of photosynthesis (Shinde et al., 2020). Our dynamic FBA simulations in COMETS
527 (Figure S5) showed similar growth between Δ*gnd* and the wild type and slightly lower growth for Δ*glgC*.
528 We set out to compare these observations with available experimental data. Since genetic tools for the
529 modification of *Prochlorococcus* are still lacking (Laurenceau et al., 2020), we chose data from the
530 closely related cyanobacteria *Synechococcus* as recent work described the impact of Δ*glgC* and Δ*gnd* on
531 its growth during diel cycles (Shinde et al., 2020). Indeed, we found very good agreement between
532 measured and predicted growth for both the wild-type and Δ*glgC* mutant where glycogen storage is
533 disrupted (Shinde et al., 2020) (Figure S5). One of the notable limitations of dynamic FBA is the ability to
534 quantify intermediates and precursor pools that might drive the initiation of a pathway. This comes
535 mainly from the assumption of a quasi steady-state of intracellular metabolite pools at each time point.
536 Although the comparison is strictly qualitative and concerns strains with known differences (Mary et al.,

2004), these findings demonstrated the ability of our reconstruction to capture metabolic trends in response to genetic perturbations, indicating that *i*SO595 will be a valuable tool in future research of *Prochloroccus.* Overall, our dynamic simulations display biological and physiological behaviors that are consistent with expectations, and at the same time provide valuable insight into the putative internal metabolic processes that might modulate the *Prochlorococcus* growth under environmental and genome-induced constraints.

Conclusions

Our study provides a detailed systematic view of the underlying metabolic trends modulating carbon storage and exudation in *Prochlorococcus*. *Prochlorococcus* is known to interact with other bacteria in its surroundings (Sher et al., 2011; Aharonovich and Sher, 2016; Biller et al., 2018; Hennon et al., 2018). It is currently impossible to predict the fluxes of organic matter (or of the myriad metabolites comprising it, such as amino acids, sugars and organic acids) between phytoplankton and bacteria. Yet, quantifying such fluxes and predicting them from genomic surveys, as shown here, serves a number of roles: (1) It can provide experimentally testable and mechanistic hypotheses on inter-microbial exchanges and competition, (2) It has the potential to increase knowledge about the specific metabolites that may mediate these interactions; and (3) It would enable the construction of improved models of biogeochemical cycles which consider the diverse and powerful metabolic capabilities of the ocean microbiome.

Genome-scale metabolic-network reconstructions are a powerful tool, but not without limitations. With the development of an innovative semi-automated approach (the ReFill algorithm), we were able to increase existing knowledge in the reconstruction by up to 25%. In contrast to other standard gap filling approaches (Henry et al., 2010; Thiele et al., 2014), or plain addition of newly found reactions, ReFill has the specific capability to add individual reactions through a recursive algorithm that guarantees

complete connectivity to the existing network. However, this approach employs high stringency and thus adds limited amounts of knowledge. Considering that *Prochlorococcus* strains have some of the smallest known genomes among free-living organisms, a 25% increase in knowledge serves as a significant improvement in the predictive capacity of the model. However, reconstruction of high-quality genome-scale metabolic models is an iterative process, where new data, knowledge, and scope creates a demand and possibility for further model improvement. One example of this possibility is the CO_2 concentrating mechanisms in *Prochlorococcus.* This mechanism is known to be sustained by proton and ion gradients across the cell membrane at an energetic cost (Hopkinson et al., 2014; Burnap et al., 2015). However, the comprehensive knowledge and annotation of ion transporters necessary to model this mechanism are lacking, and therefore, not included in iSO595. With the advancement of data collection and annotation tools, together with using ReFill or similar algorithms, metabolic knowledge can be easily added to such reconstructions and improve their predictive abilities and mimicry of biological and physiological processes. Our findings contribute to a growing body of work on the underlying metabolic mechanisms modulating the metabolic success of *Prochlorococcus*. The approaches shown here provide systematic insights corroborated in recent and well-known works and provide strong foundations for future studies of *Prochlorococcus* metabolism with particular interest in its interaction with other microorganisms and the effects of these on community composition and larger biogeochemical cycles.

Acknowledgments

This work is available as preprint on bioRxiv in https://doi.org/10.1101/2020.07.20.211680 (Ofaim et al., 2020)

Conflict of interest statement

The authors declare no conflict of interest.

Author contributions

DSh and DSe designed the study. SO, SS and DSe developed the computational models and performed the computational analyses. SO and SS wrote a first version of the manuscript. DSe, DSh and EA, oversaw the project and contributed to the final version of this manuscript. All authors have read and approved the final version of the manuscript.

Funding

This work was supported by the Human Frontiers Science Program (grant RGP0020/2016) and the National Science Foundation (NSFOCE-BSF 1635070) to DSe and Dsh. DSe also acknowledges support by the National Science Foundation (grants 1457695), the Directorates for Biological Sciences and Geosciences at the National Science Foundation and NASA (agreement nos. 80NSSC17K0295, 80NSSC17K0296 and 1724150) issued through the Astrobiology Program of the Science Mission Directorate, and the Boston University Interdisciplinary Biomedical Research Office. SS was funded by SINTEF, the Norwegian graduate research school in bioinformatics, biostatistics and systems biology (NORBIS) and by the INBioPharm project of the Centre for Digital Life Norway (Research Council of Norway grant no. 248885).

Supplemental material

604 **Figure S1: Estimation of kinetic parameters for the uptake of ammonium in *Prochlorococcus.* A)** All
605 combinations of Km and Vmax along the red trajectory matches the observed gross growth rate of 0.5 d^{-1}
606 (Grossowicz et al., 2017). However, when we compare the dynamics of cell density **(B)** and ammonium
607 concentration **(C)** we find that the best overall prediction is achieved using Km = 0.39 mM and Vmax =
608 0.9 mmol gDW^{-1} h^{-1} (marked by an orange dot in **A**).
609
610 **Figure S2: ATP availability influence modulates the trade-off between glycogen storage and growth.**
611 Phenotypic phase planes (Edwards et al., 2002) illustrate the combined effect of glycogen storage and
612 bicarbonate uptake on the maximal growth rate. Compared to the base model **(A)**, we observe how that
613 the trade-off is strongly affected by modulated ATP availability, either from an artificial reaction
614 providing extra ATP **(B)** or by increasing **(C)** or decreasing **(D)** the amount of available light. Increasing
615 ATP allows more glycogen storage without reducing the growth rate.
616
617 **Figure S3: TCA cycle flux diagram differences between the most common phenotypes.** Flux diagrams of
618 the TCA cycle in the most common phenotypes 2 (colored orange) and 3 (colored blue). Reactions are
619 denoted by KEGG reaction ids. Reaction colors correspond to cluster colors presented in figure 4.
620
621 **Figure S4: The transition from daytime to nighttime is associated with a drastic change in the**
622 **production and consumption of the energy-carrying cofactors. The figure panels show the major**
623 **sources (left) and drains (right) of the cofactors ATP, NAPDH and NADH.** The legend shows the reaction
624 IDs used in iSO595. **A)** ATP is produced by both the thylakoid (R00086th) and the periplasmic (R00086p)
625 ATP synthase during daytime, but mostly by the periplasmic ATP synthase (respiration) during nighttime.
626 ATP is consumed by reactions associated with growth (BIOMASS and BProtein), cellular maintenance
627 (Maintenance) and storage of glycogen (R00948) in addition to reactions recycling precursors for the

628 Calvin cycle (R01512 and R01523) and acetyl-CoA carboxylase (R00742). **B)** NADPH is produced by
629 ferredoxin reductase (fdr) during daytime and by the pentose phosphate pathway (R02736 and R01528)
630 during nighttime. The NADPH is either used to drive the proton gradient across the periplasmic
631 membrane (NADPHDHp) or in Gluconeogenesis (R01063) to refuel the Calvin cycle during
632 photosynthesis. **C)** NADH production is correlated with the growth rate and dominated by pyruvate
633 dehydrogenase (R00209) during daytime and the glycine cleavage system (R01221) during nighttime.
634 NADH is consumed by 6-phosphogluconate dehydrogenase (reverse, R10221) during daytime, NADH
635 transhydrogenase (R00112) solely during dusk and concomitant with methylenetetrahydrofolate
636 reductase (R07168) during nighttime.
637
638 **Figure S5: Predicted growth curves show good agreement in a qualitative comparison with**
639 **experimental growth of *Synechococcus.*** To compare growth data we have overlaid growth curves
640 predicted for the wild-type, the *ΔglgC*-mutant and the *Δgnd*-mutant of *Prochlorococcus* with
641 experimental OD measurements of *Synechococcus elongatus PCC 794* (Shinde et al., 2020). We find a
642 very good agreement for the wild-type and *ΔglgC*-mutant, but not for the *Δgnd*-mutant. The lower panel
643 shows how the model predicts the allocation and consumption of each of the three strains.
644 **Table S1:** List of reactions added to iJC568 to form iSO595.
645 **Table S2:** List of reactions from iJC568 that are modified in iSO595.
646 **Table S3:** Parameter ranges used in the sampling of nutrient environments.
647 **Table S4:** List of blocked exchange reactions prior to sampling of nutrient environments.
648 **Table S5:** Parameter values used to run dynamic FBA in COMETS.
649 **Supplemental material 1:** Results from the BLAST-search used to identify 6PG-dehydratase (EC:
650 4.2.1.12) encoded by PMM0774 in *P. marinus* MED4.
651 **Supplemental material 2:** memote snapshot report of *i*SO595.

Figure legends

Figure 1: iSO595 is an updated reconstruction of *P. marinus* MED4, featuring a complete Entner-Doudoroff pathway, rewired glycogen metabolism and increased coverage of the genome. The central panel is a simplified illustration covering the most relevant metabolic features. **A)** To simulate the natural environmental constraints experience by Prochlorococcus we use "Push-FBA": Light and bicarbonate uptake is given a fixed flux independent of growth rate. This contrasts standard FBA where light and bicarbonate would be "pulled" in by the demand needed to support maximal growth rate up to a given bound. **B)** We rewired the glycogen metabolism in iSO595 to study the dynamic allocation the dynamic allocation of glycogen. **C)** Additionally, we implemented dynamic light conditions and light absorption in COMETS to simulate the growth of *P. marinus* during the diel cycle. **D)** iSO595 has increased coverage both in terms of genes, reactions and metabolites compared to its ancestor iJC568.

Figure 2: Schematic description of the ReFill algorithm. New reaction annotations are added only if all the metabolites are connected to the existing network. A connected metabolite is denoted in a green circle. An orphan (unconnected metabolite is denoted in a red circle) (A) A simple case in which all the metabolites comply with the selection rule. (B) In case one or more metabolites are not connected to the existing network, other new reactions may be added to complete the missing connections. For example, consider reaction a to be composed of two substrates and two products, one of which, x (a metabolite that did not exist in the initial network), is not connected to the existing network and is currently an orphan. After the expansion step, the algorithm identified one reaction, b, in which x is

675 used as a substrate. All other metabolites in b exist in the network thus creating a path from reaction a
676 through reaction b to the network.

677
678 **Figure 3:** Histograms of environmental sampling results provide insight into how the fixed uptake rates
679 of light and bicarbonate and the upper bounds on ammonium and phosphate affects exudation of
680 organic acids, nucleobases and nucleotides, amino acids as well as glycogen storage. The y-axis
681 represents the fraction of all sampled environments yielding feasible models. Although we initially
682 sample each parameter uniformly the final sample distribution is not uniform because some
683 combination of parameters represents infeasible phenotypes (no solution can satisfy the constraints).
684 The final sample distribution for each parameter is therefore shown in the figure panels as a blue line.
685 The black and red line represents the histograms of samples where exudation is predicted by FBA and
686 pFBA, respectively. The shaded green region represents the span between histograms of samples as
687 predicted by FVA: the lower and upper bound represents the number of samples where exudation is
688 predicted using the minimum and maximum value of FVA, respectively. This FVA region covers the range
689 of possible phenotypes. The lower bound of the FVA region display the number of samples where a
690 certain outcome is obligatory to maximize growth, while the upper bound of the FVA region display the
691 number of samples where the outcome is possibly without reducing growth.

692 **Figure 4:** T-SNE clustering identifies typical phenotypes from the pFBA results from the random samples.
693 **A)** The random samples are reduced into two dimensions with t-SNE. We have subsequently used
694 HDBSCAN to identify 6 disjoint clusters which represents different phenotypes. **B)** For each of the 6
695 clusters the mean uptake or exudation across all samples within the respective cluster is shown. Only
696 exchange reactions with an absolute flux above 1e-3 mmol gDW^{-1} h^{-1} in any of the random samples are
697 included.

Figure 5: Correlation between maximal FVA values demonstrate which compounds that can be secreted in similar environmental conditions. There are two clearly correlated groups of compounds: The first group comprises nucleobases, nucleotides and amino acids while the second contains organic acids, glycogen and glycerol 3-phosphate. From the correlation of each of these groups with the uptake bounds on ammonium and phosphate we observe that these factors determine which of the groups that can be secreted. Note that the environmental constraints have been converted to positive values prior to calculating the correlation.

Figure 6: Insight into metabolic rearrangements during the diel cycle. **A)** Light irradiance, biomass and glycogen storage throughout the diel cycle. We observe that the largest accumulated growth is found in the nitrogen-abundant condition (green), but glycogen is only predicted to be stored in the nitrogen-poor condition (orange). **B)** The flux distributions shifts when the metabolism switches from photosynthesis to glycogen catabolism, displayed by five reactions representing the Calvin Cycle (CBB), Glycogen metabolism, lower part of glycolysis, The Entner-Doudoroff (ED) and the Penthose Phosphate Pathway (PPP). **C)** iSO595 predicts that the depletion of glycogen is accompanied by exudation of fumarate and pyruvate.

References

Aharonovich, D., and Sher, D. (2016). Transcriptional response of Prochlorococcus to co-culture with a marine Alteromonas: Differences between strains and the involvement of putative infochemicals. *ISME J.* 10, 2892–2906. doi:10.1038/ismej.2016.70.

Altschul, S., Gish, W., Miller, W., Myers, E., and Lipman, D. (1990). Basic local alignment search tool. *J Mol Biol* 215. doi:10.1016/S0022-2836(05)80360-2.

Amin, S. A., Parker, M. S., and Armbrust, E. V. (2012). Interactions between Diatoms and Bacteria. 76, 667–684. doi:10.1128/MMBR.00007-12.

Arrieta, J. M., Mayol, E., Hansman, R. L., and Herndl, G. J. (2015). Dilution limits dissolved organic carbon utilization in the deep ocean. 348, 331–334.

Becker, J. W., Berube, P. M., Follett, C. L., Waterbury, J. B., Chisholm, S. W., Delong, E. F., et al. (2014). Closely related phytoplankton species produce similar suites of dissolved organic matter. 5, 1–14. doi:10.3389/fmicb.2014.00111.

Benson, P. J., Purcell-Meyerink, D., Hocart, C. H., Truong, T. T., James, G. O., Rourke, L., et al. (2016). Factors Altering Pyruvate Excretion in a Glycogen Storage Mutant of the Cyanobacterium, Synechococcus PCC7942. *Front. Microbiol.* 7, 475. doi:10.3389/fmicb.2016.00475.

Bertilsson, S., and Berglund, O. (2014). Release of dissolved organic matter by Prochlorococcus RELEASE OF DISSOLVED ORGANIC MATTER BY.

Biller, S. J., Berube, P. M., Lindell, D., and Chisholm, S. W. (2015). Prochlorococcus: The structure and function of collective diversity. *Nat. Rev. Microbiol.* 13, 13–27. doi:10.1038/nrmicro3378.

Biller, S. J., Coe, A., Roggensack, S. E., and Chisholm, W. (2018). Heterotroph Interactions Alter Prochlorococcus Transcriptome. 3, 1–18.

Braakman, R. (2019). Evolution of cellular metabolism and the rise of a globally productive biosphere. *Free Radic. Biol. Med.* 140, 172–187. doi:10.1016/j.freeradbiomed.2019.05.004.

Braakman, R., Follows, M. J., and Chisholm, S. W. (2017). Metabolic evolution and the self-organization of ecosystems. *Proc. Natl. Acad. Sci.* 114, E3091–E3100. doi:10.1073/pnas.1619573114.

Bricaud, A., Claustre, H., Ras, J., and Oubelkheir, K. (2004). Natural variability of phytoplanktonic absorption in oceanic waters: Influence of the size structure of algal populations. *J. Geophys. Res.*

Ocean. 109, 1–12. doi:10.1029/2004JC002419.

Broddrick, J. T., Rubin, B. E., Welkie, D. G., Du, N., Mih, N., Diamond, S., et al. (2016). Unique attributes of cyanobacterial metabolism revealed by improved genome-scale metabolic modeling and essential gene analysis. *Proc. Natl. Acad. Sci.* 113, E8344–E8353. doi:10.1073/pnas.1613446113.

Burnap, R., Hagemann, M., and Kaplan, A. (2015). Regulation of CO2 Concentrating Mechanism in Cyanobacteria. *Life* 5, 348–371. doi:10.3390/life5010348.

Campillo-Brocal, J. C., Lucas-Elió, P., and Sanchez-Amat, A. (2015). Distribution in different organisms of amino acid oxidases with fad or a quinone as cofactor and their role as antimicrobial proteins in marine bacteria. *Mar. Drugs* 13, 7403–7418. doi:10.3390/md13127073.

Cano, M., Holland, S. C., Artier, J., Burnap, R. L., Ghirardi, M., Morgan, J. A., et al. (2018). Glycogen Synthesis and Metabolite Overflow Contribute to Energy Balancing in Cyanobacteria. *Cell Rep.* 23, 667–672. doi:10.1016/j.celrep.2018.03.083.

Carrieri, D., Paddock, T., Maness, P.-C., Seibert, M., and Yu, J. (2012). Photo-catalytic conversion of carbon dioxide to organic acids by a recombinant cyanobacterium incapable of glycogen storage. *Energy Environ. Sci.* 5, 9457. doi:10.1039/c2ee23181f.

Casey, J. R., Mardinoglu, A., Nielsen, J., and Karl, D. M. (2016). Adaptive Evolution of Phosphorus Metabolism in Prochlorococcus. *mSystems* 1, 1–15. doi:10.1128/mSystems.00065-16.Editor.

Chen, X., Schreiber, K., Appel, J., Makowka, A., Fähnrich, B., Roettger, M., et al. (2016). The Entner-Doudoroff pathway is an overlooked glycolytic route in cyanobacteria and plants. *Proc. Natl. Acad. Sci. U. S. A.* 113, 5441–5446. doi:10.1073/pnas.1521916113.

Cirri, E., and Pohnert, G. (2019). Algae–bacteria interactions that balance the planktonic microbiome. *New Phytol.* 223, 100–106. doi:10.1111/nph.15765.

Coles, V. J., Stukel, M. R., Brooks, M. T., Burd, A., Crump, B. C., Moran, M. A., et al. (2017). Ocean biogeochemistry modeled with emergent trait-based genomics. *Science (80-.).* 358, 1149–1154.

doi:10.1126/science.aan5712.

Damrow, R., Maldener, I., and Zilliges, Y. (2016). The multiple functions of common microbial carbon polymers, glycogen and PHB, during stress responses in the non-diazotrophic cyanobacterium synechocystis sp. PCC 6803. *Front. Microbiol.* 7, 1–10. doi:10.3389/fmicb.2016.00966.

Davey, M., Tarran, G. A., Mills, M. M., Ridame, C., Geider, R. J., and LaRoche, J. (2008). Nutrient limitation of picophytoplankton photosynthesis and growth in the tropical North Atlantic. *Limnol. Oceanogr.* 53, 1722–1733. doi:10.4319/lo.2008.53.5.1722.

de Groot, D. H., Lischke, J., Muolo, R., Planqué, R., Bruggeman, F. J., and Teusink, B. (2020). The common message of constraint-based optimization approaches: overflow metabolism is caused by two growth-limiting constraints. *Cell. Mol. Life Sci.* 77, 441–453. doi:10.1007/s00018-019-03380-2.

Diamond, S., Jun, D., Rubin, B. E., and Golden, S. S. (2015). The circadian oscillator in Synechococcus elongatus controls metabolite partitioning during diurnal growth. *Proc. Natl. Acad. Sci. U. S. A.* 112, E1916–E1925. doi:10.1073/pnas.1504576112.

Díaz-Troya, S., López-Maury, L., Sánchez-Riego, A. M., Roldán, M., and Florencio, F. J. (2014). Redox regulation of glycogen biosynthesis in the cyanobacterium synechocystis sp. PCC 6803: Analysis of the AGP and glycogen synthases. *Mol. Plant* 7, 87–100. doi:10.1093/mp/sst137.

Domínguez-Martín, M. A., López-Lozano, A., Clavería-Gimeno, R., Velázquez-Campoy, A., Seidel, G., Burkovski, A., et al. (2018). Differential NtcA responsiveness to 2-oxoglutarate underlies the diversity of C/N balance regulation in Prochlorococcus. *Front. Microbiol.* 8, 1–16. doi:10.3389/fmicb.2017.02641.

Dubinsky, Z., and Berman-Frank, I. (2001). Uncoupling primary production from population growth in photosynthesizing organisms in aquatic ecosystems. in *Aquatic Sciences* (Birkhauser Verlag AG), 4–17. doi:10.1007/PL00001343.

Ebrahim, A., Lerman, J. A., Palsson, B. O., and Hyduke, D. R. (2013). COBRApy: COnstraints-Based

Reconstruction and Analysis for Python. *BMC Syst. Biol.* 7, 74. doi:10.1186/1752-0509-7-74.

Edwards, J. S., Ramakrishna, R., and Palsson, B. O. (2002). Characterizing the metabolic phenotype: A phenotype phase plane analysis. *Biotechnol. Bioeng.* 77, 27–36. doi:10.1002/bit.10047.

Elbourne, L. D. H., Tetu, S. G., Hassan, K. A., and Paulsen, I. T. (2017). TransportDB 2.0: A database for exploring membrane transporters in sequenced genomes from all domains of life. *Nucleic Acids Res.* 45, D320–D324. doi:10.1093/nar/gkw1068.

Feist, A. M., Nagarajan, H., Rotaru, A. E., Tremblay, P. L., Zhang, T., Nevin, K. P., et al. (2014). Constraint-Based Modeling of Carbon Fixation and the Energetics of Electron Transfer in Geobacter metallireducens. *PLoS Comput. Biol.* 10. doi:10.1371/journal.pcbi.1003575.

Field, C. B., Behrenfeld, M. J., Randerson, J. T., and Falkowski, P. (1998). Primary production of the biosphere: Integrating terrestrial and oceanic components. *Science (80-.).* 281, 237–240. doi:10.1126/science.281.5374.237.

Flombaum, P., Gallegos, J. L., Gordillo, R. A., Rincón, J., Zabala, L. L., Jiao, N., et al. (2013a). Present and future global distributions of the marine Cyanobacteria Prochlorococcus and Synechococcus. *Proc. Natl. Acad. Sci. U. S. A.* 110, 9824–9829. doi:10.1073/pnas.1307701110.

Flombaum, P., Gallegos, J. L., Gordillo, R. A., Rincón, J., Zabala, L. L., Jiao, N., et al. (2013b). Present and future global distributions of the marine Cyanobacteria Prochlorococcus and Synechococcus. *Proc. Natl. Acad. Sci. U. S. A.* 110, 9824–9829. doi:10.1073/pnas.1307701110.

Follows, M. J., Dutkiewicz, S., Grant, S., and Chisholm, S. W. (2007). Emergent Biogeography of Microbial. *Science (80-.).*, 1843–1847. doi:10.1126/science.1138544.

Forchhammer, K., and Schwarz, R. (2019). Nitrogen chlorosis in unicellular cyanobacteria – a developmental program for surviving nitrogen deprivation. *Environ. Microbiol.* 21, 1173–1184. doi:10.1111/1462-2920.14447.

Forchhammer, K., and Selim, K. A. (2019). Carbon/nitrogen homeostasis control in cyanobacteria. *FEMS*

Microbiol. Rev. 44, 33–53. doi:10.1093/femsre/fuz025.

Foster, S. Q., Al-haj, A., Church, M. J., Dijken, G. L. Van, Dutkiewicz, S., Fulweiler, R. W., et al. (2018). Ecological control of nitrite in the upper ocean. *Nat. Commun.* doi:10.1038/s41467-018-03553-w.

Gilbert, J. D. J., and Fagan, W. F. (2011). Contrasting mechanisms of proteomic nitrogen thrift in Prochlorococcus. *Mol. Ecol.* 20, 92–104. doi:10.1111/j.1365-294X.2010.04914.x.

Gomez, J. A., Höffner, K., and Barton, P. I. (2014). DFBAlab: A fast and reliable MATLAB code for dynamic flux balance analysis. *BMC Bioinformatics* 15, 409. doi:10.1186/s12859-014-0409-8.

Grossowicz, M., Roth-Rosenberg, D., Aharonovich, D., Silverman, J., Follows, M. J., and Sher, D. (2017). *Prochlorococcus* in the lab and in silico: The importance of representing exudation. *Limnol. Oceanogr.* 62, 818–835. doi:10.1002/lno.10463.

Gu, C., Kim, G. B., Kim, W. J., Kim, H. U., and Lee, S. Y. (2019). Current status and applications of genome-scale metabolic models. *Genome Biol.* 20, 1–18. doi:10.1186/s13059-019-1730-3.

Gudmundsson, S., and Thiele, I. (2010). Computationally efficient flux variability analysis. *BMC Bioinformatics* 11, 489. doi:10.1186/1471-2105-11-489.

Harcombe, W. R., Riehl, W. J., Dukovski, I., Granger, B. R., Betts, A., Lang, A. H., et al. (2014). Metabolic resource allocation in individual microbes determines ecosystem interactions and spatial dynamics. *Cell Rep.* 7, 1104–1115. doi:10.1016/j.celrep.2014.03.070.

Haug, K., Salek, R. M., Conesa, P., Hastings, J., De Matos, P., Rijnbeek, M., et al. (2013). MetaboLights - An open-access general-purpose repository for metabolomics studies and associated meta-data. *Nucleic Acids Res.* 41, 781–786. doi:10.1093/nar/gks1004.

Hennon, G. M., Morris, J. J., Haley, S. T., Zinser, E. R., Durrant, A. R., Entwistle, E., et al. (2018). The impact of elevated CO 2 on Prochlorococcus and microbial interactions with â € helper' bacterium Alteromonas. *ISME J.* 12, 520–531. doi:10.1038/ismej.2017.189.

Henry, C. S., Dejongh, M., Best, A. A., Frybarger, P. M., Linsay, B., and Stevens, R. L. (2010). High-

842 throughput generation, optimization and analysis of genome-scale metabolic models. *Nat.*
843 *Biotechnol.* 28, 977–982. doi:10.1038/nbt.1672.
844 Holtzendorff, J., Partensky, F., Mella, D., Lennon, J.-F., Hess, W. R., and Garczarek, L. (2008). Genome
845 Streamlining Results in Loss of Robustness of the Circadian Clock in the Marine Cyanobacterium
846 *Prochlorococcus marinus* PCC 9511. *J. Biol. Rhythms* 23, 187–199. doi:10.1177/0748730408316040.
847 Hopkinson, B. M., Young, J. N., Tansik, A. L., and Binder, B. J. (2014). The minimal CO2-concentrating
848 mechanism of prochlorococcus spp. MED4 is effective and efficient. *Plant Physiol.* 166, 2205–2217.
849 doi:10.1104/pp.114.247049.
850 Iglesias, A. A., Kakefuda, G., and Preiss, J. (1991). Regulatory and structural properties of the
851 cyanobacterial ADPglucose pyrophosphorylases. *Plant Physiol.* 97, 1187–1195.
852 doi:10.1104/pp.97.3.1187.
853 Johnson, Z. I., Zinser, E. R., Coe, A., McNulty, N. P., Woodward, E. M. S., and Chisholm, S. W. (2006).
854 Niche partitioning among Prochlorococcus ecotypes along ocean-scale environmental gradients.
855 *Science (80-.).* 311, 1737–1740. doi:10.1126/science.1118052.
856 Kanehisa, M., and Goto, S. (2000). KEGG: kyoto encyclopedia of genes and genomes. *Nucleic Acids Res.*
857 28, 27–30. Available at: http://www.ncbi.nlm.nih.gov/pubmed/10592173 [Accessed October 23,
858 2017].
859 Kavvas, E. S., Seif, Y., Yurkovich, J. T., Norsigian, C., Poudel, S., Greenwald, W. W., et al. (2018). Updated
860 and standardized genome-scale reconstruction of Mycobacterium tuberculosis H37Rv, iEK1011,
861 simulates flux states indicative of physiological conditions. *BMC Syst. Biol.* 12. doi:10.1186/s12918-
862 018-0557-y.
863 Kim, J., Fabris, M., Baart, G., Kim, M. K., Goossens, A., Vyverman, W., et al. (2016). Flux balance analysis
864 of primary metabolism in the diatom *Phaeodactylum tricornutum*. *Plant J.* 85, 161–176.
865 doi:10.1111/tpj.13081.

Knoop, H., Gründel, M., Zilliges, Y., Lehmann, R., Hoffmann, S., Lockau, W., et al. (2013). Flux Balance Analysis of Cyanobacterial Metabolism: The Metabolic Network of Synechocystis sp. PCC 6803. *PLoS Comput. Biol.* 9. doi:10.1371/journal.pcbi.1003081.

Krumhardt, K. M., Callnan, K., Roache-Johnson, K., Swett, T., Robinson, D., Reistetter, E. N., et al. (2013). Effects of phosphorus starvation versus limitation on the marine cyanobacterium ProchlorococcusMED4 I: Uptake physiology. *Environ. Microbiol.* 15, 2114–2128. doi:10.1111/1462-2920.12079.

Kujawinski, E. B. (2011). The Impact of Microbial Metabolism on Marine Dissolved Organic Matter. doi:10.1146/annurev-marine-120308-081003.

Laurenceau, R., Bliem, C., Osburne, M. S., Becker, J. W., Biller, S. J., Cubillos-Ruiz, A., et al. (2020). Toward a genetic system in the marine cyanobacterium Prochlorococcus. *Access Microbiol.* 2, e000107. doi:10.1099/acmi.0.000107.

Lewis, N. E., Hixson, K. K., Conrad, T. M., Lerman, J. A., Charusanti, P., Polpitiya, A. D., et al. (2010). Omic data from evolved *E. coli* are consistent with computed optimal growth from genome-scale models. *Mol. Syst. Biol.* 6, 390. doi:10.1038/msb.2010.47.

Lieven, C., Beber, M. E., Olivier, B. G., Bergmann, F. T., Ataman, M., Babaei, P., et al. (2020). MEMOTE for standardized genome-scale metabolic model testing. *Nat. Biotechnol.* 38, 272–276. doi:10.1038/s41587-020-0446-y.

Long, S. P., Humphries, S., and Falkowski, P. G. (1994). Photoinhibition of Photosynthesis in Nature. *Annu. Rev. Plant Physiol. Plant Mol. Biol.* 45, 633–662. doi:10.1146/annurev.pp.45.060194.003221.

Luan, G., Zhang, S., Wang, M., and Lu, X. (2019). Progress and perspective on cyanobacterial glycogen metabolism engineering. *Biotechnol. Adv.* 37, 771–786. doi:10.1016/j.biotechadv.2019.04.005.

Ma, L., Calfee, B. C., Morris, J. J., Johnson, Z. I., and Zinser, E. R. (2018a). Degradation of hydrogen peroxide at the ocean's surface: The influence of the microbial community on the realized thermal

niche of Prochlorococcus. *ISME J.* 12, 473–484. doi:10.1038/ismej.2017.182.

Ma, X., Coleman, M. L., and Waldbauer, J. R. (2018b). Distinct molecular signatures in dissolved organic matter produced by viral lysis of marine cyanobacteria. *Environ. Microbiol.* 20, 3001–3011. doi:10.1111/1462-2920.14338.

Maarleveld, T. R., Khandelwal, R. A., Olivier, B. G., Teusink, B., and Bruggeman, F. J. (2013). Basic concepts and principles of stoichiometric modeling of metabolic networks. *Biotechnol. J.* 8, 997–1008. doi:10.1002/biot.201200291.

Maaten, L. van der, and Hinton, G. (2008). Visualizing data using t-SNE. *J. Mach. Learn. Res.* 9, 2579–2605.

Mahadevan, R., Edwards, J. S., and Doyle, F. J. (2002). Dynamic Flux Balance Analysis of diauxic growth in Escherichia coli. *Biophys. J.* 83, 1331–1340. doi:10.1016/S0006-3495(02)73903-9.

Mary, I., Tu, C.-J., Grossman, A., and Vaulot, D. (2004). Effects of high light on transcripts of stress-associated genes for the cyanobacteria Synechocystis sp. PCC 6803 and Prochlorococcus MED4 and MIT9313. *Microbiology* 150, 1271–1281. doi:10.1099/mic.0.27014-0.

McInnes, L., Healy, J., and Astels, S. (2017). hdbscan: Hierarchical density based clustering. *J. Open Source Softw.* 2, 205. doi:10.21105/joss.00205.

McKinney, W. (2010). pandas: a Foundational Python Library for Data Analysis and Statistics | R (Programming Language) | Database Index. Available at: https://www.scribd.com/document/71048089/pandas-a-Foundational-Python-Library-for-Data-Analysis-and-Statistics [Accessed April 29, 2020].

Monk, J. M., Lloyd, C. J., Brunk, E., Mih, N., Sastry, A., King, Z., et al. (2017). iML1515, a knowledgebase that computes Escherichia coli traits. *Nat. Biotechnol.* 35, 904–908. doi:10.1038/nbt.3956.

Moore, C. M., Mills, M. M., Arrigo, K. R., Berman-Frank, I., Bopp, L., Boyd, P. W., et al. (2013). Processes and patterns of oceanic nutrient limitation. *Nat. Geosci.* 6, 701–710. doi:10.1038/ngeo1765.

Moore, L. R., Coe, A., Zinser, E. R., Saito, M. A., Sullivan, M. B., Lindell, D., et al. (2007). Culturing the marine cyanobacterium Prochlorococcus. *Limnol. Oceanogr. Methods* 5, 353–362. doi:10.4319/lom.2007.5.353.

Moradi, N., Liu, B., Iversen, M., and Kuypers, M. M. (2018). A new mathematical model to explore microbial processes and their constraints in phytoplankton colonies and sinking marine aggregates. 1–10.

Moran, M. A., and Durham, B. P. (2019). Sulfur metabolites in the pelagic ocean. *Nat. Rev. Microbiol.* 17, 665–678. doi:10.1038/s41579-019-0250-1.

Moran, M. A., Kujawinski, E. B., Stubbins, A., Fatland, R., Aluwihare, L. I., Buchan, A., et al. (2016). Deciphering ocean carbon in a changing world. *Proc. Natl. Acad. Sci.* 113, 3143–3151. doi:10.1073/pnas.1514645113.

Morel, A., and Bricaud, A. (1981). Theoretical results concerning light absorption in a discrete medium, and application to specific absorption of phytoplankton. *Deep Sea Res. Part A, Oceanogr. Res. Pap.* 28, 1375–1393. doi:10.1016/0198-0149(81)90039-X.

Morris, J. J., Lenski, R. E., and Zinser, E. R. (2012). The black queen hypothesis: Evolution of dependencies through adaptive gene loss. *MBio* 3. doi:10.1128/mBio.00036-12.

Muñoz-Marín, M. C., Gómez-Baena, G., López-Lozano, A., Moreno-Cabezuelo, J. A., Díez, J., and García-Fernández, J. M. (2020). Mixotrophy in marine picocyanobacteria: use of organic compounds by Prochlorococcus and Synechococcus. *ISME J.* 14, 1065–1073. doi:10.1038/s41396-020-0603-9.

Nogales, J., Gudmundsson, S., Knight, E. M., Palsson, B. O., and Thiele, I. (2012). Detailing the optimality of photosynthesis in cyanobacteria through systems biology analysis. *Proc. Natl. Acad. Sci. U. S. A.* 109, 2678–2683. doi:10.1073/pnas.1117907109.

Noreña-Caro, D., and Benton, M. G. (2018). Cyanobacteria as photoautotrophic biofactories of high-value chemicals. *J. CO2 Util.* 28, 335–366. doi:10.1016/j.jcou.2018.10.008.

O'Brien, E. J., Monk, J. M., and Palsson, B. O. (2015). Using genome-scale models to predict biological capabilities. *Cell* 161, 971–987. doi:10.1016/j.cell.2015.05.019.

Ofaim, S., Sulheim, S., Almaas, E., Sher, D., and Segrè, D. (2020). Dynamic allocation of carbon storage and nutrient-dependent exudation in a revised genome-scale model of Prochlorococcus. Cold Spring Harbor Laboratory doi:10.1101/2020.07.20.211680.

Orth, J. D., Thiele, I., and Palsson, B. O. (2010). What is flux balance analysis? *Nat. Biotechnol.* 28, 245–248. doi:10.1038/nbt.1614.

Pacheco, A. R., Moel, M., and Segrè, D. (2018). Costless metabolic secretions as drivers of interspecies interactions in microbial ecosystems. 1–42.

Park, J., and Choi, Y. (2017). Cofactor engineering in cyanobacteria to overcome imbalance between NADPH and NADH: A mini review. *Front. Chem. Sci. Eng.* 11, 66–71. doi:10.1007/s11705-016-1591-1.

Partensky, F., and Garczarek, L. (2010). *Prochlorococcus*: Advantages and Limits of Minimalism. *Ann. Rev. Mar. Sci.* 2, 305–331. doi:10.1146/annurev-marine-120308-081034.

Partensky, F., Hess, W. R., and Vaulot, D. (1999). Prochlorococcus, a Marine Photosynthetic Prokaryote of Global Significance. *Microbiol. Mol. Biol. Rev.* 63, 106–127. doi:10.1128/mmbr.63.1.106-127.1999.

Pedregosa, F., Varoquaux, G., Gramfort, A., Michel, V., Thirion, B., Grisel, O., et al. (2011). Scikit-learn: Machine Learning in Python. *J. Mach. Learn. Res.* 12, 2825–2830. Available at: http://jmlr.org/papers/v12/pedregosa11a.html.

Reid, A. (2011). Incorporating Microbial Processes into Climate Change Models. 2–32.

Reimers, A.-M., Knoop, H., Bockmayr, A., and Steuer, R. (2017). Cellular trade-offs and optimal resource allocation during cyanobacterial diurnal growth. *Proc. Natl. Acad. Sci.*, 201617508. doi:10.1073/pnas.1617508114.

Ribalet, F., Swalwell, J., Clayton, S., Jiménez, V., Sudek, S., Lin, Y., et al. (2015). Light-driven synchrony of Prochlorococcus growth and mortality in the subtropical Pacific gyre. *Proc. Natl. Acad. Sci. U. S. A.* 112, 8008–12. doi:10.1073/pnas.1424279112.

Roth-rosenberg, D., Aharonovich, D., Omta, A.-W., Follows, M. J., and Sciences, P. (2019). Dynamic macromolecular composition and high exudation rates in Prochlorococcus. *bioRxiv*, 828897. doi:10.1101/828897.

Saito, M. A., McIlvin, M. R., Moran, D. M., Goepfert, T. J., DiTullio, G. R., Post, A. F., et al. (2014). Multiple nutrient stresses at intersecting Pacific Ocean biomes detected by protein biomarkers. *Science (80-.).* 345, 1173–1177. doi:10.1126/science.1256450.

Seaver, L. C., and Imlay, J. A. (2001). Hydrogen peroxide fluxes and compartmentalization inside growing Escherichia coli. *J. Bacteriol.* 183, 7182–7189. doi:10.1128/JB.183.24.7182-7189.2001.

Sher, D., Thompson, J. W., Kashtan, N., Croal, L., and Chisholm, S. W. (2011). Response of Prochlorococcus ecotypes to co-culture with diverse marine bacteria. *ISME J.* 5, 1125–1132. doi:10.1038/ismej.2011.1.

Shinde, S., Zhang, X., Singapuri, S. P., Kalra, I., Liu, X., Morgan-Kiss, R. M., et al. (2020). Glycogen Metabolism Supports Photosynthesis Start through the Oxidative Pentose Phosphate Pathway in Cyanobacteria. *Plant Physiol.* 182, 507–517. doi:10.1104/pp.19.01184.

Sosa, O. A., Casey, J. R., and Karl, D. M. (2019). Methylphosphonate Oxidation in Prochlorococcus Strain MIT9301 Supports Phosphate Acquisition, Formate Excretion, and Carbon Assimilation into Purines. *Appl. Environ. Microbiol.* 85. doi:10.1128/AEM.00289-19.

Szul, M. J., Dearth, S. P., Campagna, S. R., and Zinser, E. R. (2019). Carbon Fate and Flux in Prochlorococcus under Nitrogen Limitation . *mSystems* 4. doi:10.1128/msystems.00254-18.

Thiele, I., Hyduke, D. R., Steeb, B., Fankam, G., Allen, D. K., Bazzani, S., et al. (2011). A community effort towards a knowledge-base and mathematical model of the human pathogen Salmonella

Typhimurium LT2. *BMC Syst. Biol.* 5. doi:10.1186/1752-0509-5-8.

Thiele, I., Vlassis, N., and Fleming, R. M. T. (2014). FASTGAPFILL: Efficient gap filling in metabolic networks. *Bioinformatics* 30, 2529–2531. doi:10.1093/bioinformatics/btu321.

Thornton, D. C. O. (2014). Dissolved organic matter (DOM) release by phytoplankton in the contemporary and future ocean Dissolved organic matter (DOM) release by phytoplankton in the contemporary and future ocean. *Eur. J. Phycol.* 49, 20–46. doi:10.1080/09670262.2013.875596.

Van Mooy, B. A. S., Rocap, G., Fredricks, H. F., Evans, C. T., and Devol, A. H. (2006). Sulfolipids dramatically decrease phosphorus demand by picocyanobacteria in oligotrophic marine environments. *Proc. Natl. Acad. Sci. U. S. A.* 103, 8607–8612. doi:10.1073/pnas.0600540103.

Varma, A., and Palsson, B. O. (1994). Metabolic flux balancing: Basic concepts, scientific and practical use. *Bio/Technology* 12, 994–998. doi:10.1038/nbt1094-994.

Vaulot, D., Marie, D., Olson, R. J., and Chisholm, S. W. (1995). Growth of Prochlorococcus, a photosynthetic prokaryote, in the equatorial Pacific Ocean. *Science (80-.).* 268, 1480–1482. doi:10.1126/science.268.5216.1480.

Virtanen, P., Gommers, R., Oliphant, T. E., Haberland, M., Reddy, T., Cournapeau, D., et al. (2020). SciPy 1.0: fundamental algorithms for scientific computing in Python. *Nat. Methods* 17, 261–272. doi:10.1038/s41592-019-0686-2.

Waldbauer, J. R., Rodrigue, S., Coleman, M. L., and Chisholm, S. W. (2012). Transcriptome and Proteome Dynamics of a Light-Dark Synchronized Bacterial Cell Cycle. *PLoS One* 7, e43432. doi:10.1371/journal.pone.0043432.

Welkie, D. G., Rubin, B. E., Diamond, S., Hood, R. D., Savage, D. F., and Golden, S. S. (2019). A Hard Day ' s Night : Cyanobacteria in Diel Cycles. 27, 231–242.

Xiong, W., Cano, M., Wang, B., Douchi, D., and Yu, J. (2017). The plasticity of cyanobacterial carbon metabolism. *Curr. Opin. Chem. Biol.* 41, 12–19. doi:10.1016/j.cbpa.2017.09.004.

Yang, A. (2011). Modeling and evaluation of CO 2 supply and utilization in algal ponds. *Ind. Eng. Chem. Res.* 50, 11181–11192. doi:10.1021/ie200723w.

Yoshikawa, K., Toya, Y., and Shimizu, H. (2017). Metabolic engineering of Synechocystis sp. PCC 6803 for enhanced ethanol production based on flux balance analysis. *Bioprocess Biosyst. Eng.* 40, 791–796. doi:10.1007/s00449-017-1744-8.

Zhang, C. C., Zhou, C. Z., Burnap, R. L., and Peng, L. (2018). Carbon/Nitrogen Metabolic Balance: Lessons from Cyanobacteria. *Trends Plant Sci.* 23, 1116–1130. doi:10.1016/j.tplants.2018.09.008.

Zinser, E. R., Lindell, D., Johnson, Z. I., Futschik, M. E., Steglich, C., Coleman, M. L., et al. (2009). Choreography of the transcriptome, photophysiology, and cell cycle of a minimal photoautotroph, Prochlorococcus. *PLoS One* 4. doi:10.1371/journal.pone.0005135.

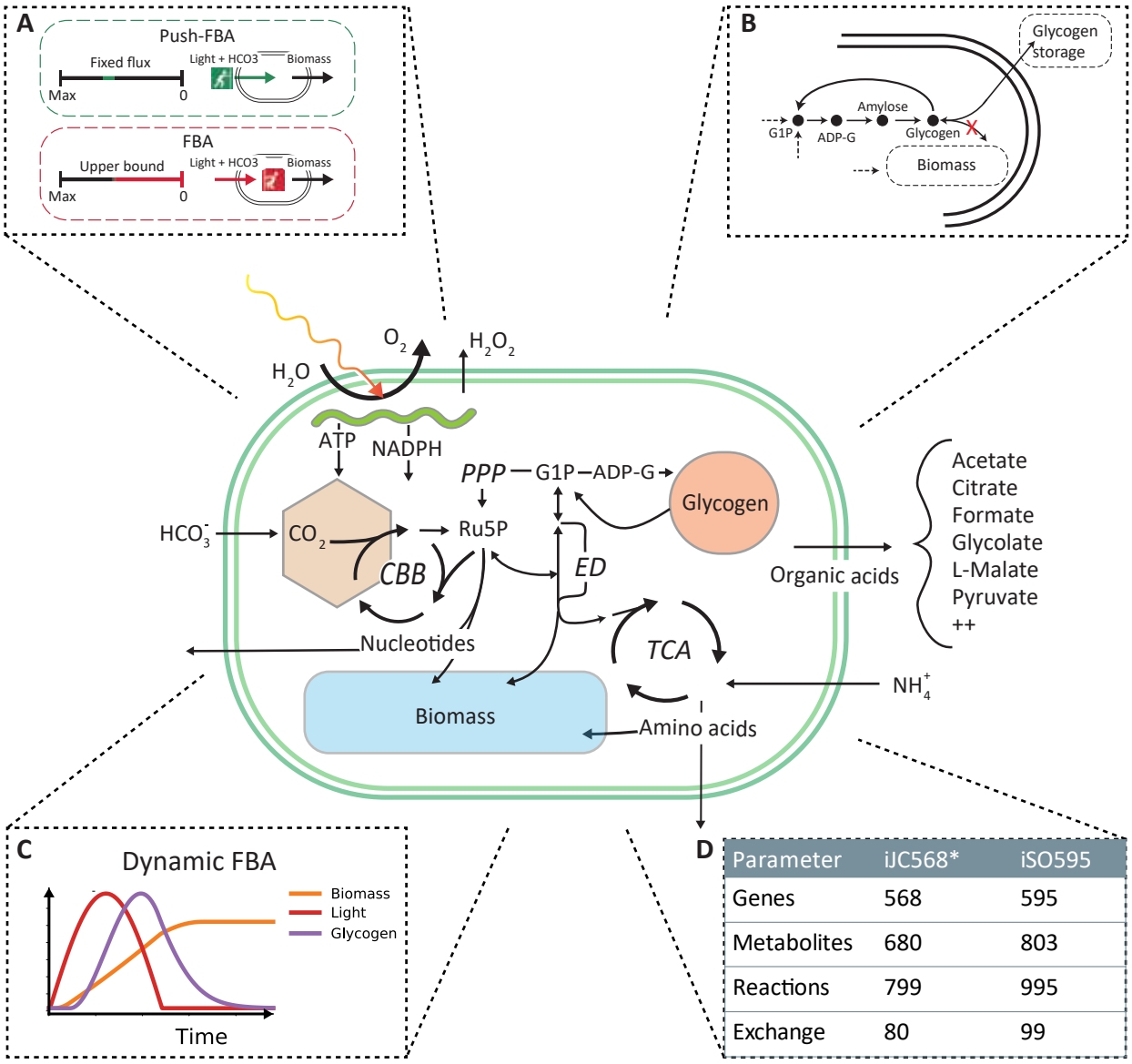

Parameter	iJC568*	iSO595
Genes	568	595
Metabolites	680	803
Reactions	799	995
Exchange	80	99

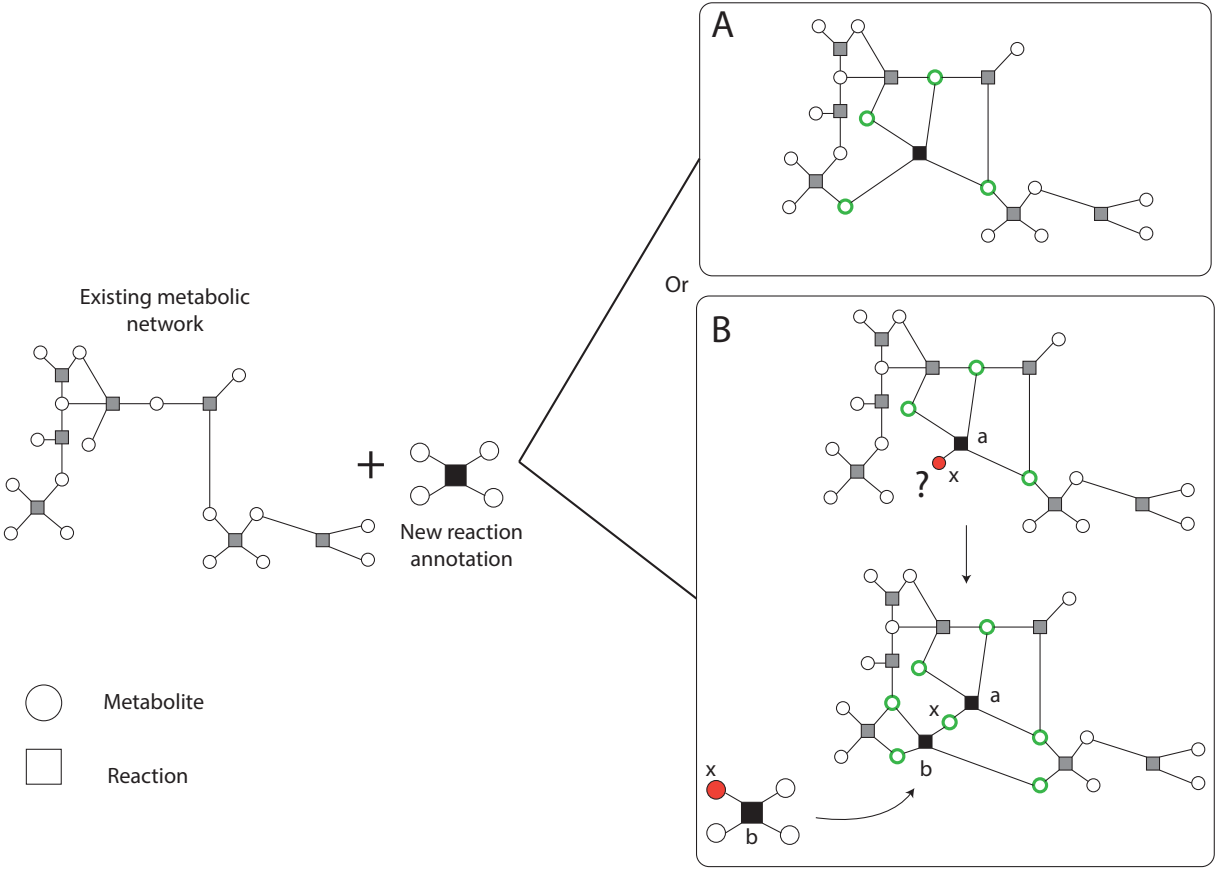
Existing metabolic network
+
New reaction annotation
Metabolite
Reaction
Or
A
B
a
x
?
x
a
b
x
b

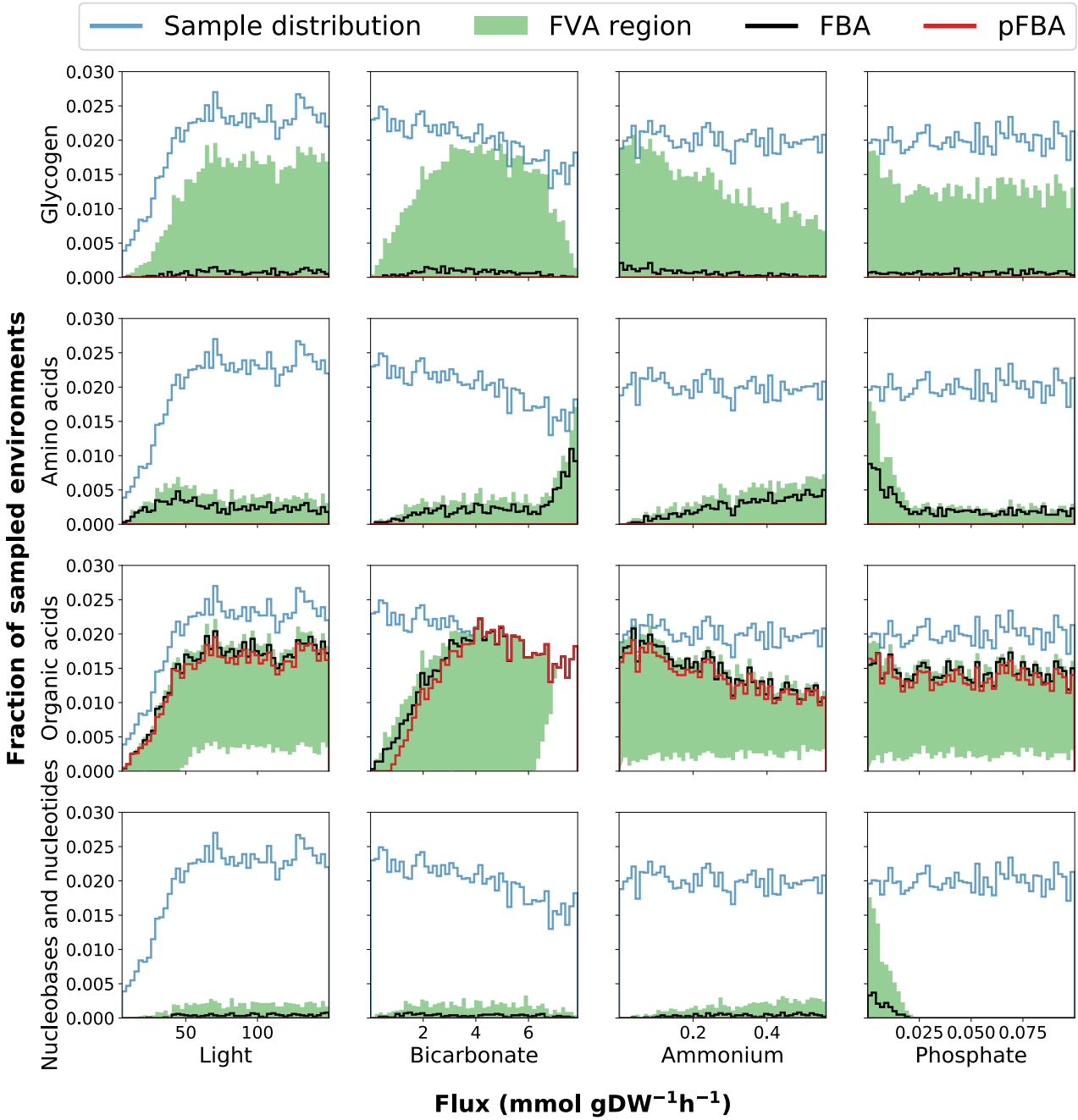
Sample distribution
FVA region
FBA
pFBA
Fraction of sampled environments
Glycogen
Amino acids
Organic acids
Nucleobases and nucleotides
0.030
0.025
0.020
0.015
0.010
0.005
0.000
50
100
Light
2
4
6
Bicarbonate
0.2
0.4
Ammonium
0.025
0.050
0.075
Phosphate
Flux (mmol gDW^{-1}h^{-1})

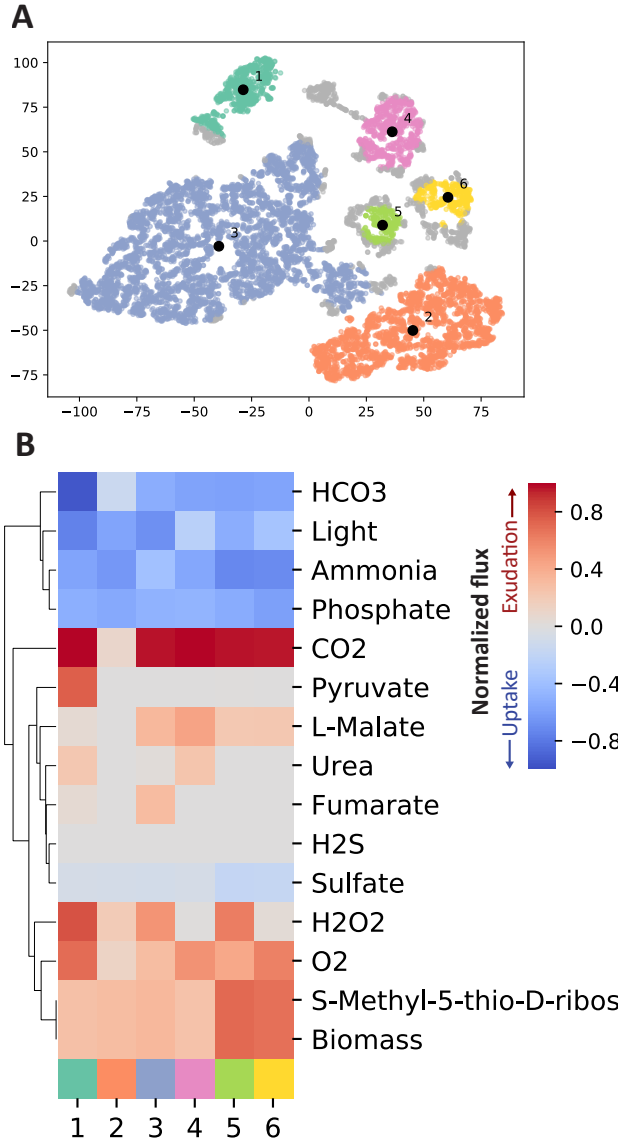
A
100
75
50
25
0
−25
−50
−75
−100
−75
−50
−25
0
25
50
75
1
2
3
4
5
6
B
HCO3
Light
Ammonia
Phosphate
CO2
Pyruvate
L-Malate
Urea
Fumarate
H2S
Sulfate
H2O2
O2
S-Methyl-5-thio-D-ribose
Biomass
1
2
3
4
5
6
Normalized flux
Exudation
Uptake
0.8
0.4
0.0
−0.4
−0.8

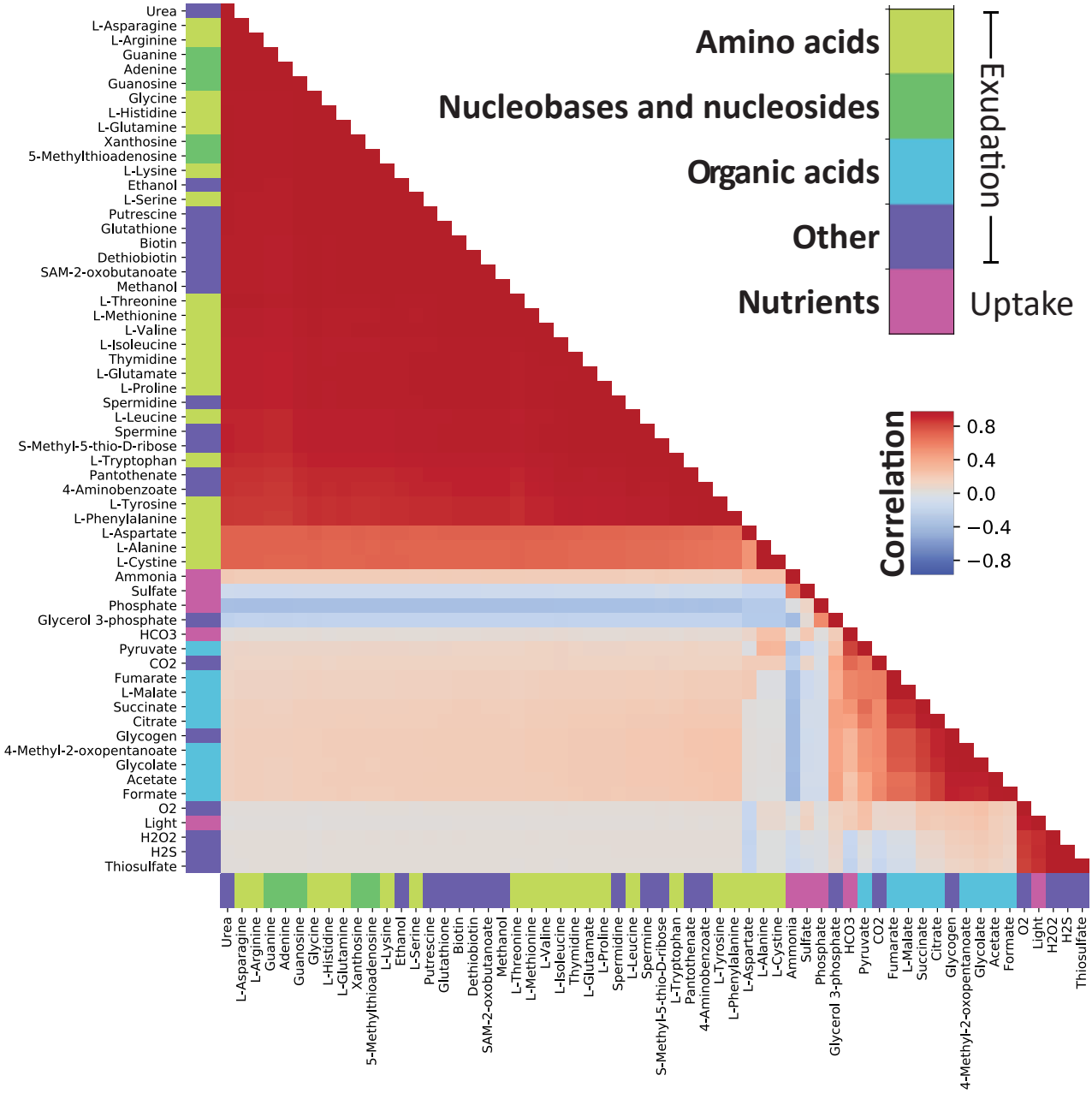
Amino acids
Nucleobases and nucleosides
Organic acids
Other
Nutrients
Exudation
Uptake
Correlation
0.8
0.4
0.0
−0.4
−0.8
Urea
L-Asparagine
L-Arginine
Guanine
Adenine
Guanosine
Glycine
L-Histidine
L-Glutamine
Xanthosine
5-Methylthioadenosine
L-Lysine
Ethanol
L-Serine
Putrescine
Glutathione
Biotin
Dethiobiotin
SAM-2-oxobutanoate
Methanol
L-Threonine
L-Methionine
L-Valine
L-Isoleucine
Thymidine
L-Glutamate
L-Proline
Spermidine
L-Leucine
Spermine
S-Methyl-5-thio-D-ribose
L-Tryptophan
Pantothenate
4-Aminobenzoate
L-Tyrosine
L-Phenylalanine
L-Aspartate
L-Alanine
L-Cystine
Ammonia
Sulfate
Phosphate
Glycerol 3-phosphate
HCO3
Pyruvate
CO2
Fumarate
L-Malate
Succinate
Citrate
Glycogen
4-Methyl-2-oxopentanoate
Glycolate
Acetate
Formate
O2
Light
H2O2
H2S
Thiosulfate

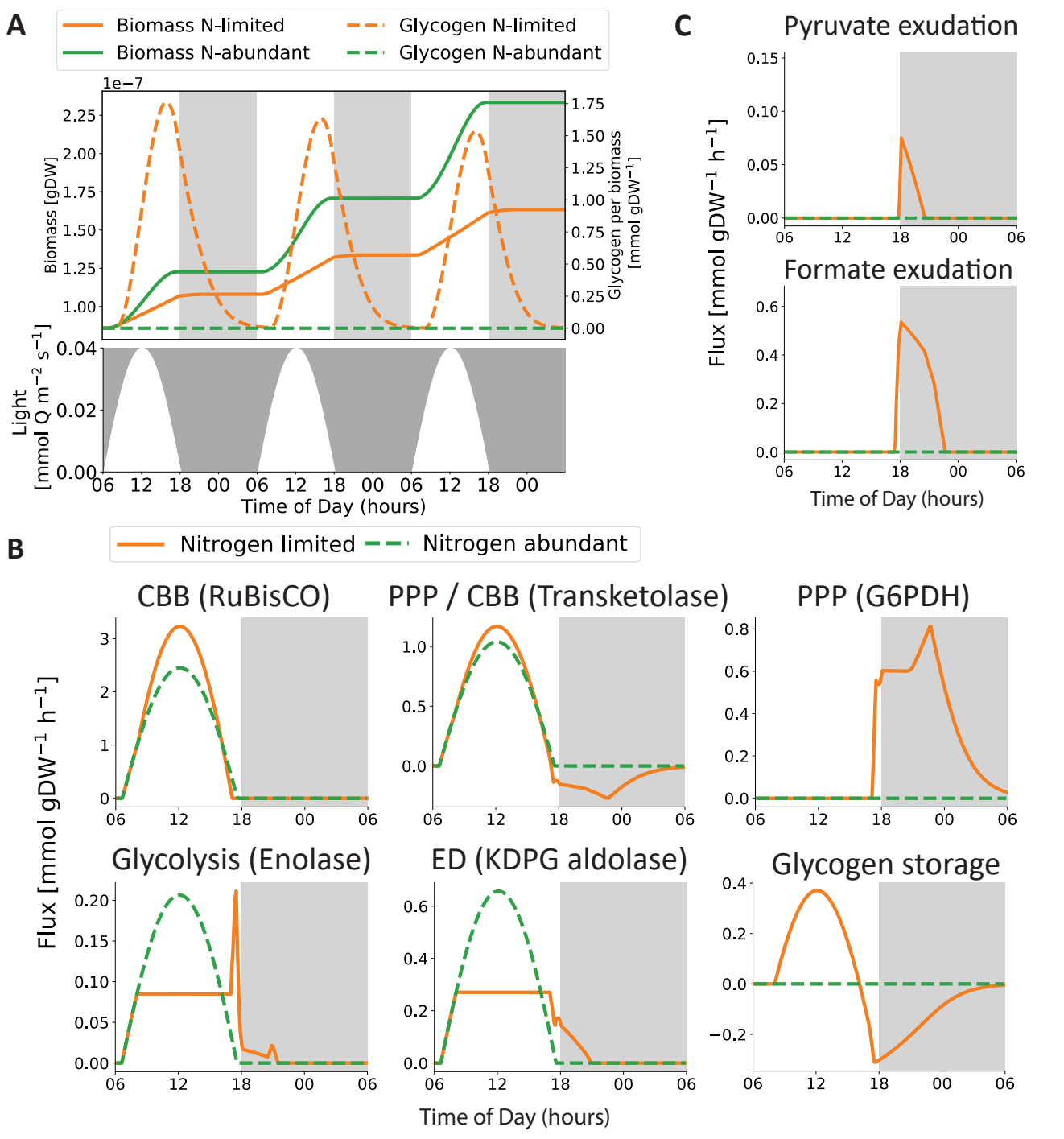
A
Biomass N-limited
Biomass N-abundant
Glycogen N-limited
Glycogen N-abundant
1e−7
Biomass [gDW]
Glycogen per biomass [mmol gDW^{-1}]
Light [mmol Q m^{-2} s^{-1}]
Time of Day (hours)
C
Pyruvate exudation
Formate exudation
Flux [mmol gDW^{-1} h^{-1}]
Time of Day (hours)
B
Nitrogen limited
Nitrogen abundant
CBB (RuBisCO)
PPP / CBB (Transketolase)
PPP (G6PDH)
Glycolysis (Enolase)
ED (KDPG aldolase)
Glycogen storage
Flux [mmol gDW^{-1} h^{-1}]
Time of Day (hours)